

Peristaltic Pumping of Blood Through Small Vessels of Varying Cross-section

J.C.Misra^{1*}, S. Maiti^{2†}

¹*Professor, Department of Mathematics,*

Institute of Technical Education and Research,

Siksha O Anusandhan University, Bhubaneswar-751030, India

²*School of Medical Science and Technology & Center for Theoretical Studies,
Indian Institute of Technology, Kharagpur-721302, India*

Abstract

The paper is devoted to a study of the peristaltic motion of blood in the micro-circulatory system. The vessel is considered to be of varying cross-section. The progressive peristaltic waves are taken to be of sinusoidal nature. Blood is considered to be a Herschel-Bulkley fluid. Of particular concern here is to investigate the effects of amplitude ratio, mean pressure gradient, yield stress and the power law index on the velocity distribution, streamline pattern and wall shear stress. On the basis of the derived analytical expression, extensive numerical calculations have been made. The study reveals that velocity of blood and wall shear stress are appreciably affected due to the non-uniform geometry of blood vessels. They are also highly sensitive to the magnitude of the amplitude ratio and the value of the fluid index.

Keywords: Non-Newtonian Fluid, Retrograde Flow, Wall Shear Stress, Trajectory.

1 Introduction

Peristaltic transport is well known to physiologists as a natural mechanism of pumping materials in the case of most physiological fluids. Apart from physiological fluids, some other fluids also exhibit peristaltic behaviour. Peristalsis usually occurs when the flow is induced by a

*Email address: *misrajc@rediffmail.com (J. C. Misra)*

†Email address: *somnathm@cts.iitkgp.ernet.in (S. Maiti)*

progressive wave of area contraction/expansion along the length of the boundary of a fluid-filled distensible tube. Usefulness of studies on peristaltic flow has been discussed in detail in our earlier publications (Misra et al. [1, 2, 3, 4, 5, 6, 7, 8, 9], Maiti and Misra [10, 11]) and in some other references [12, 13].

Nomenclature	
a_0	Half-width of the channel at the inlet
b	Wave amplitude
H	Vertical displacement of the wall
n	Flow index number
n_1	Reciprocal of n
P	Fluid pressure
\bar{Q}	Flux at axial location
t	Time
X, Y	Rectangular Cartesian co-ordinates
U, V	Velocity components in X,Y directions respectively
δ	Wave number
Δp	Pressure difference between the channel ends
λ	Wave length of the travelling wave motion of the wall
Λ	A parametric constant
μ	Blood viscosity
ν	Kinematic viscosity of blood
ϕ	Amplitude ratio
ρ	Density of blood
τ_0	Yield stress of blood
τ_h	Wall shear stress

The phenomenon of peristalsis plays an important role in the functioning of heart-lung machine, blood pump machine and dialysis machine. Fung and Yih [14] presented a theoretical analysis of peristaltic transport primarily with inertia-free Newtonian flows driven by sinusoidal transverse waves of small amplitude. Investigation of peristaltic motion in connection with functions of different physiological systems such as the ureter, the gastro-intestinal tract, the small blood vessels and other glandular ducts was first made by Shapiro et al. [15]. They presented a closed form solution for an infinite train of waves for small Reynolds number flow. Their study was,

however, restricted to cases where the wave length is long and the wave amplitude is arbitrary. Conditions for the the presence of physiologically significant phenomena of trapping and reflux were also suggested by them. Jaffrin and Shapiro [13] as well as Srivastava and Srivastava [16] summarized the early literatures on peristaltic transport. Some of the recent studies on peristaltic transport were discussed by Usha and Rao [17], Mishra and Rao [18], Yaniv et al. [19], Jimenez-Lozano et al [20], Wang et al. [21] and Hayat et al. [22].

Some important theoretical analyses on different aspects of blood flow were carried out in a systematic manner by Misra et al. [23, 24, 25]. Attempt to consider the complex rheology of various physiological fluids was made in several studies [26, 27, 28, 29, 30, 31, 32, 33, 34]. The non-Newtonian behaviour of blood mainly owes to the presence of erythrocytes in whole blood. In the case of blood, such behaviour starts becoming prominent when the hematocrit rises above 20%. This particular behaviour plays a dominating role when the hematocrit level lies between 40% and 70% [35, 36, 37]. Some other relevant theoretical studies on non-Newtonian fluid flows were carried out by Masud and Kwack [38], Kwack and Masud [39] as well as by Anand and Rajagopal [40].

It is known that the flow behaviour of blood in small vessels (diameter < 0.02 cm) and at low shear rate ($< 20 \text{sec}^{-1}$) can be represented by a power law fluid [41, 42]. Merrill et al. [43] pointed out that Casson model holds satisfactory for blood flowing in tubes of $130\text{-}1000 \mu\text{m}$. Moreover, Blair and Spanner [44] reported that blood obeys Casson model for moderate shear rate flows. However, they pointed out that for cow's blood, Herschel-Bulkley model is more appropriate than Casson model.

It is known that physiological organs are by and large non-uniform ducts [45, 46, 47]. Several authors [16, 48, 49] made some initial attempts to perform theoretical studies pertaining to peristaltic transport of physiological fluids in vessels of non-uniform cross section. These analyses were mostly restricted to the assumption of either a Newtonian fluid or a non-Newtonian fluid of Casson/power-law type. Moreover, in these reports the different flow characteristics have not been adequately discussed. The strong merit of Herschel-Bulkley model is that fluids represented by this model describe very well material flows with a non-linear constitutive relation depicting the behaviour of shear-thinning/shear-thickening fluids that are of much importance in the field of biomedical engineering [50]. It is also to be noted that for formulating a non-Newtonian model of blood, Herschel-Bulkley fluid model is more general than most other non-Newtonian fluid models. It is worthwhile to mention that results for a fluid represented by Bingham plastic model, power law model and Newtonian fluid model can be derived from those of the Herschel-

Bulkley fluid model. Also this model has been found to yield more accurate results than many other non-Newtonian models.

In view of the above, we have taken up here a study on the peristaltic transport of blood in a non-uniform channel, by treating blood as a Herschel-Bulkley fluid. It is worthwhile to mention that flow through axisymmetric tubes is qualitatively similar to the case of flow in channels. On the basis of their theoretical/experimental study on peristaltic pumping at low Reynolds number, Shapiro et al. [15] also confirmed that flow behaviour in the case of an axisymmetric tube is identical to that in the case of channel flow. The formulation and analysis presented in the sequel are particularly suitable for investigating the peristaltic motion in vessels of small dimensions, e.g. arterioles and venules. Since for flow of blood through smaller vessels in the micro-circulatory system, the Reynolds number is low and since the ratio between half-width of the channel under consideration and the wave length is considered small, it has been possible to perform the theoretical analysis for the present problem in a convenient manner, by using the lubrication theory [15]. On the basis of the derived analytical expressions, computational work has been executed keeping a specific situation of micro-circulation in view, with the main purpose of examining the distribution of velocity of blood and wall shear stress as well as the streamline pattern, trajectories of individual fluid particles and pumping performance. The plots for the computed results give us a clear idea of qualitative variation of various fluid dynamical parameters. The results indicate plug flow in the central region, where most of the erythrocytes are accumulated and non-plug flow in the peripheral region. The results of the present study are in good agreement with those reported earlier by previous investigators. The study bears the potential to explore some important phenomena that are useful for having a better insight into the flow in the micro-circulatory system.

The study has an important bearing on the clinical procedure of extra-corporeal circulation of blood by using the heart-lung machine, where there is a chance of damage of erythrocytes owing to significant variation of the wall shear stress. The results are also likely to find important application in roller pumps and arthro-pumps by which fluids can be transported in living organs in pathological states.

2 Formulation and Analysis

Let us consider the peristaltic motion of blood, by treating it as an incompressible viscous non-Newtonian fluid. The non-Newtonian behaviour is considered to be of Herschel-Bulkley type.

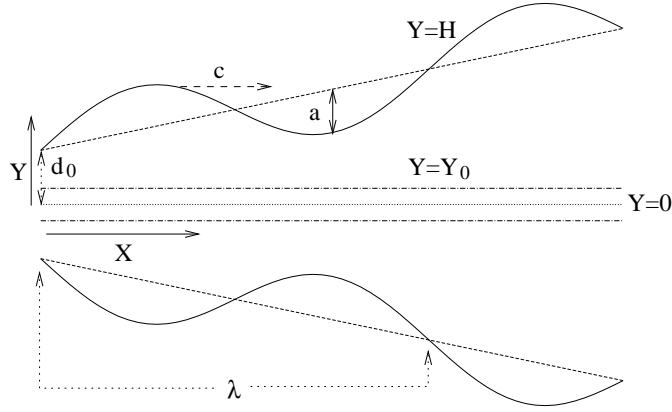


Figure 1: A physical sketch of the problem for a tapered channel

We shall study two-dimensional channel flow, width of the channel being non-uniform.

We take (X, Y) as Cartesian coordinates of the location of a fluid particle, X being measured in the direction of wave propagation and Y in the normal direction. Let $Y = H$ and $Y = -H$ be respectively the upper and lower boundaries of the channel (cf. Fig. 1). The medium is considered to be induced by a progressive sinusoidal wave train propagating with a constant speed c along the channel wall, such that $H = d(X) + a \sin(\frac{2\pi}{\lambda}(X - ct))$, with $d(X) = d_0 + \Lambda X$. $d(X)$ represents the half-width of the channel at any axial distance X from the inlet, d_0 being the half-width at the inlet, $\Lambda (< 1)$ a constant whose magnitude depends on the length of the channel as well as the inlet and outlet dimensions, a the wave amplitude, t the time and λ the wave length.

Under the assumptions stated above, the basic equations that govern the fluid motion are the field equations

$$\nabla \cdot \mathbf{V} = 0$$

$$\text{and } \rho \frac{d\mathbf{V}}{dt} = \nabla \cdot \sigma + \rho \mathbf{f},$$

where \mathbf{V} is the velocity, \mathbf{f} the body force per unit mass and ρ the density of the fluid, while $\frac{d}{dt}$ denotes the material time derivative. σ is the Cauchy stress defined by $\sigma = -PI + T$, where $T = 2\mu E_{ij} + \eta IS$ and $S = \nabla \cdot \mathbf{V}$, E_{ij} being the symmetric part of the velocity gradient L , $E_{ij} = \frac{1}{2}[L + L^T]$, $L = \nabla \mathbf{V}$.

$-PI$ denotes the indeterminate part of the stress due to the constraint of incompressibility; μ and η are viscosity parameters. The Herschel-Bulkley model gives the combined effect of

Bingham plastic and power-law behavior of a fluid. At low strain rate ($\dot{\gamma} < \frac{\tau_0}{\mu_0}$), the material acts like a viscous fluid with constant viscosity μ_0 . But when the strain rate increases and the yield stress threshold, τ_0 , is reached, the fluid behavior is described by a power law

$$\mu = \frac{\tau_0 + \alpha \left\{ \dot{\gamma}^n - \left(\frac{\tau_0}{\mu_0} \right)^n \right\}}{\dot{\gamma}},$$

where α and n denote respectively the consistency factors and the power law index. $n < 1$ and $n > 1$ correspond to a shear thinning fluid and a shear thickening fluid respectively. If the channel length is an integral multiple of the wavelength, the pressure difference across the ends of the channel is a constant. The pressure p remains constant across any axial station of the channel, when the wavelength is large and curvature effects are negligibly small. Since in the study, the geometry of wall surface is non-uniform, the flow is inherently unsteady in the laboratory frame as well as in the wave frame of reference. Disregarding the body forces (i.e. taking $f=0$), and using the Herschel-Bulkley equations, the governing equations of the incompressible fluid motion in the micro-vessel in the fixed frame of reference may be put in the form

$$\rho \left(\frac{\partial U}{\partial t} + U \frac{\partial U}{\partial X} + V \frac{\partial U}{\partial Y} \right) = - \frac{\partial P}{\partial X} + \frac{\partial \tau_{XX}}{\partial X} + \frac{\partial \tau_{XY}}{\partial Y} \quad (1)$$

$$\rho \left(\frac{\partial V}{\partial t} + U \frac{\partial V}{\partial X} + V \frac{\partial V}{\partial Y} \right) = - \frac{\partial P}{\partial Y} + \frac{\partial \tau_{YX}}{\partial X} + \frac{\partial \tau_{YY}}{\partial Y} \quad (2)$$

$$\text{with } \tau_{ij} = 2\mu E_{ij} = \mu \left(\frac{\partial U_i}{\partial X_j} + \frac{\partial U_j}{\partial X_i} \right), \quad (3)$$

$$\mu = \begin{cases} \mu_0 & : \text{ for } \Pi \leq \Pi_0, \\ \alpha \Pi^{n-1} + \tau_0 \Pi^{-1} & : \text{ for } \Pi \geq \Pi_0 \end{cases} \quad (4)$$

$$\Pi = \sqrt{2E_{ij}E_{ij}} \quad (5)$$

The limiting viscosity μ_0 is considered such that

$$\mu_0 = \alpha \Pi_0^{n-1} + \tau_0 \Pi_0^{-1} \quad (6)$$

In the analysis that follows, we shall make use of the following non-dimensional variables:

$$\begin{aligned} \bar{X} &= \frac{X}{\lambda}, \quad \bar{Y} = \frac{Y}{d_0}, \quad \bar{U} = \frac{U}{c}, \quad \bar{V} = \frac{V}{c\delta}, \quad \delta = \frac{d_0}{\lambda}, \quad \bar{P} = \frac{d_0^{n+1}P}{\mu c^n \lambda}, \quad \bar{t} = \frac{ct}{\lambda}, \quad h = \frac{H}{d_0}, \quad \phi = \frac{a}{d_0}, \\ \bar{\tau}_0 &= \frac{\tau_0}{\mu \left(\frac{c}{d_0} \right)^n}, \quad \bar{\tau}_{YX} = \frac{\tau_{YX}}{\mu \left(\frac{c}{d_0} \right)^n}, \quad \bar{\Psi} = \frac{\Psi}{d_0 c} \end{aligned} \quad (7)$$

The equation governing the flow of the fluid can now be written in the form (dropping the bars over the symbols)

$$Re\delta \left(\frac{\partial U}{\partial t} + U \frac{\partial U}{\partial X} + V \frac{\partial U}{\partial Y} \right) = -\frac{\partial P}{\partial X} + 2\delta^2 \frac{\partial \left(\Phi \frac{\partial U}{\partial X} \right)}{\partial X} + \frac{\partial \left(\Phi \left(\frac{\partial U}{\partial Y} + \delta^2 \frac{\partial V}{\partial X} \right) \right)}{\partial Y} \quad (8)$$

$$Re\delta^3 \left(\frac{\partial V}{\partial t} + U \frac{\partial V}{\partial X} + V \frac{\partial V}{\partial Y} \right) = -\frac{\partial P}{\partial Y} + \delta^2 \frac{\partial \left(\Phi \left(\frac{\partial U}{\partial Y} + \delta^2 \frac{\partial V}{\partial X} \right) \right)}{\partial X} + \delta^2 \frac{\partial \left(\Phi \frac{\partial V}{\partial Y} \right)}{\partial Y} \quad (9)$$

$$\begin{aligned} \text{where } \Phi = & \left| \sqrt{2\delta^2 \left\{ \left(\frac{\partial U}{\partial X} \right)^2 + \left(\frac{\partial V}{\partial Y} \right)^2 \right\} + \left(\frac{\partial U}{\partial Y} + \delta^2 \frac{\partial V}{\partial X} \right)^2} \right|^{n-1} \\ & + \tau_0 \left| \sqrt{2\delta^2 \left\{ \left(\frac{\partial U}{\partial X} \right)^2 + \left(\frac{\partial V}{\partial Y} \right)^2 \right\} + \left(\frac{\partial U}{\partial Y} + \delta^2 \frac{\partial V}{\partial X} \right)^2} \right|^{-1} \end{aligned} \quad (10)$$

Using the long wavelength approximation ($\delta \ll 1$) and the lubrication approach [15, 18], the governing equations and the boundary conditions describing the flow in the fixed frame of reference may be rewritten in terms of the dimensionless variables as

$$\frac{\partial P}{\partial X} = \frac{\partial \tau_{YX}}{\partial Y}, \quad (11)$$

$$\frac{\partial P}{\partial Y} = 0 \quad (12)$$

$$\text{where } \tau_{YX} = \left(\tau_0 + \left| \frac{\partial U}{\partial Y} \right|^n \right) \text{sgn} \left(\frac{\partial U}{\partial Y} \right) \quad (\text{cf. [51]}), \quad (13)$$

$$\Psi = 0, \quad U_Y = \Psi_{YY} = 0, \quad \tau_{YX} = 0 \text{ at } Y = 0; \quad U = \Psi_Y = 0 \text{ at } Y = h \quad (14)$$

Thus the pressure gradient $\frac{\partial P}{\partial X}$ is independent of Y. The solution of equation (11) satisfying (14) is found in the form

$$U(X, Y, t) = \begin{cases} \frac{1}{(n_1+1)P_1} [(P_1 h - \tau_0)^{n_1+1} - (P_1 Y - \tau_0)^{n_1+1}] & : \text{ if } Y \geq 0 \\ \frac{1}{(n_1+1)P_1} [(P_1 h - \tau_0)^{n_1+1} - (-P_1 Y - \tau_0)^{n_1+1}] & : \text{ if } Y < 0, \end{cases} \quad (15)$$

where $P_1 = -\frac{\partial P}{\partial X}$, $n_1 = \frac{1}{n}$. If the plug flow region be given by $Y = Y_0$,

$$U_Y = 0 \text{ at } Y = Y_0$$

$$\text{Then } Y_0 = \frac{\tau_0}{P_1}.$$

h defined in (7) stands for the non-dimensional vertical displacement. If $\tau_{YX} = \tau_h$ at $Y=h$, we find $h = \tau_h/P_1$.

$$\text{Now } \frac{Y_0}{h} = \frac{\tau_0}{\tau_h} = \tau \text{ (say)}, \quad 0 < \tau < 1 \quad (16)$$

The plug velocity is then given by

$$U_p = \frac{(P_1 h - \tau_0)^{n_1+1}}{(n_1 + 1)P_1} \quad (17)$$

Using the boundary conditions

$$\begin{aligned} \Psi_p &= 0 \text{ at } Y = 0 \\ \text{and } \Psi &= \Psi_p \text{ at } Y = Y_0, \end{aligned}$$

and integrating (15) and (17), the stream function Ψ is found to be given by

$$\Psi = \begin{cases} \frac{P_1^{n_1}}{(n_1+1)} \left[Y(h - Y_0)^{n_1+1} - \frac{(Y-\tau_0)^{n_1+2}}{n_1+2} \right] & : \text{ if } Y_0 \leq Y \leq h \\ \frac{P_1^{n_1}}{(n_1+1)} \left[Y(h - Y_0)^{n_1+1} + \frac{(-Y-\tau_0)^{n_1+2}}{n_1+2} \right] & : \text{ if } -h \leq Y \leq -Y_0, \end{cases} \quad (18)$$

$$\text{and } \Psi_p = \frac{P_1^{n_1}(h - Y_0)^{n_1+1}Y}{n_1 + 1}, \quad \text{if } -Y_0 \leq Y \leq Y_0 \quad (19)$$

The instantaneous rate of volume flow through each section, $\bar{Q}(x, t)$, is given by

$$\begin{aligned} \bar{Q}(X, t) &= \int_0^{Y_0} U_Y dY + \int_{Y_0}^h U dY \\ &= \frac{P_1^{n_1}(h - Y_0)^{n_1+1}(n_1 h + h + Y_0)}{(n_1 + 1)(n_1 + 2)}, \quad n_1 = \frac{1}{n} \end{aligned} \quad (20)$$

$$\begin{aligned} \text{Now } \frac{\partial P}{\partial X} &= - \left[\frac{\bar{Q}(X, t)(n_1 + 1)(n_1 + 2)}{(h - Y_0)^{n_1+1}(n_1 h + h + Y_0)} \right]^n \\ &= - \left[\frac{\bar{Q}(X, t)(n_1 + 1)(n_1 + 2)}{h^{n_1+2}(1 - \tau)^{n_1+1}(n_1 + 1 + \tau)} \right]^n \end{aligned} \quad (21)$$

The average pressure rise per wave length is calculated as

$$\Delta P = - \int_0^1 \int_0^1 \left(\frac{\partial P}{\partial X} \right) dx dt \quad (22)$$

In the fixed frame of reference, the expression for the non-dimensional transverse velocity V is found to be given by

$$V(X, Y, t) = \left[\left\{ \frac{n_1}{\bar{Q}^n(X, t)} - \frac{(n_1 + 1)(n_1 + 2)}{h(1 - \tau)(n_1 + 1 + \tau)} \right\} \left\{ h(1 - \tau)^{n_1 + 1} Y - \frac{h^2}{n_1 + 2} \left(\frac{Y}{h} - \tau \right)^{n_1 + 2} \right\} \right. \\ \left. + (n_1 + 1)(1 - \tau)_1^n Y \right] \times \frac{h_1^n P_1^{n_1} \{ \Lambda \lambda / d_0 + 2\pi \phi \cos(2\pi(X - t)) \}}{n_1 + 1} \quad (23)$$

It may be noted that if we put $n = 1$, $\tau = 0$, $\Lambda = 0$ in equations (15), (18), (20) and (21), the expressions reduce to those reported earlier in [15]. Our results also tally with those of [52], when the eccentricity of the elliptical motion of cilia tips is set equal to zero in their analysis for a Newtonian fluid flowing through a uniform channel. Moreover, when $n = 1$ and $Y_0 = 0$, the expression for the pressure gradient given by (21) reduces to that obtained by Gupta and Seshadri [48] for the peristaltic motion of a Newtonian fluid having constant viscosity. It may be noted that since the right hand side of equation (22) cannot be integrated in closed form, for non-uniform/uniform geometry, for further investigation of our problem, we had to resort to the use of appropriate softwares, as mentioned in the next section.

3 Computational Results and Discussion

The instantaneous rate of volume flow $\bar{Q}(X, t)$ has been assumed to be periodic in $(X - t)$ ([16, 48, 49]), so that \bar{Q} appearing in equation (22) can be expressed as

$$\bar{Q}^n(X, t) = Q^n + \phi \sin 2\pi(X - t) , \quad (24)$$

Q being the time-averaged flow flux. Due to complexity of the problem, it has not been possible to find the expression for the average pressure rise, ΔP given by (21). It has been computed numerically by using the software Mathematica.

In this section, on the basis of the present study, we shall obtain theoretical estimates of different physical quantities that are of relevance to the physiological problem of blood flow in micro-circulatory system. For this purpose, we have used the following data valid in the physiological range ([12, 16, 53, 54]): $d_0 = 10$ to $60 \mu m$, $\phi = 0.1$ to 0.9 , $\frac{d_0}{\lambda} = 0.01$ to 0.02 , $\Delta P = -300$ to 50 , $\tau = 0.0$ to 0.2 , $Q = 0$ to 2 , $n = \frac{1}{3}$ to 2 . Unlike other studies on non-uniform geometry, the value of Λ has been so chosen that for converging tubes (e.g. arterioles), the width of the outlet of one wave length is 25% less than that of the inlet, while in the case of diverging tubes (e.g. venules), the width of the outlet of one wave length is 25% more than that of inlet.

	ϕ	Our results	Results in [25]
Wave Crest	0.2	0.244	0.25
	0.3	0.338	0.344
	0.4	0.418	0.427
Wave Trough	0.2	-0.366	-0.375
	0.3	-0.627	-0.635
	0.4	-0.976	-0.984

Table 1: Comparison of the present study with those of Takabatake and Ayukawa [25] for small values of Re and δ ($n = 1$, $\tau = 0$, $\Lambda = 0$, $Q = 0$)

It is important to mention that the results presented in the sequel for shear thinning and shear thickening fluids are quite relevant for the study of blood rheology. Normal blood usually behaves like a shear thinning fluid for which with the increase in shear rate, the viscosity decreases. It has been mentioned in [54, 55, 56] that in the case of hardened red blood cell suspension, the fluid behaviour is that of a shear thickening fluid for which with the fluid viscosity is enhanced due to an elevation of the shear rate.

3.1 Velocity Distribution

Plots in Figs. 2-6 give the distribution of axial velocity in the cases of free pumping, pumping and co-pumping for different values of the amplitude ratio ϕ , flow index number n , τ , Λ . Fig. 2(a) shows that the results computed on the basis of our study for the particular case of Newtonian fluid tally well with the results reported by Shapiro et al. [15] when the amplitude ratio $\phi = 0.5$. Variation of axial velocity in the vertical direction at the wave crest and the wave trough are exhibited in Figs. 2(b,c) for different values of ϕ . In order to compare our results with those reported by Takabatake and Ayukawa [27], we have reproduced their results alongside the results computed on the basis of the present study in Table 1. From the tabulated values, one can observe that axial velocity along the central line at the wave crest and the wave trough match well with [27] when the wave number is small. Since the velocity profiles and height of the channel change with time, investigation has been made on the basis of the present study for the distribution of velocity at an interval of $T/4$. Figs. 3 depict the aerial view of a few typical axial velocity distributions for a Newtonian fluid flowing over a uniform channel. The corresponding velocity contours for the peristaltic motion corresponding to $\phi = 0.1$ are shown in

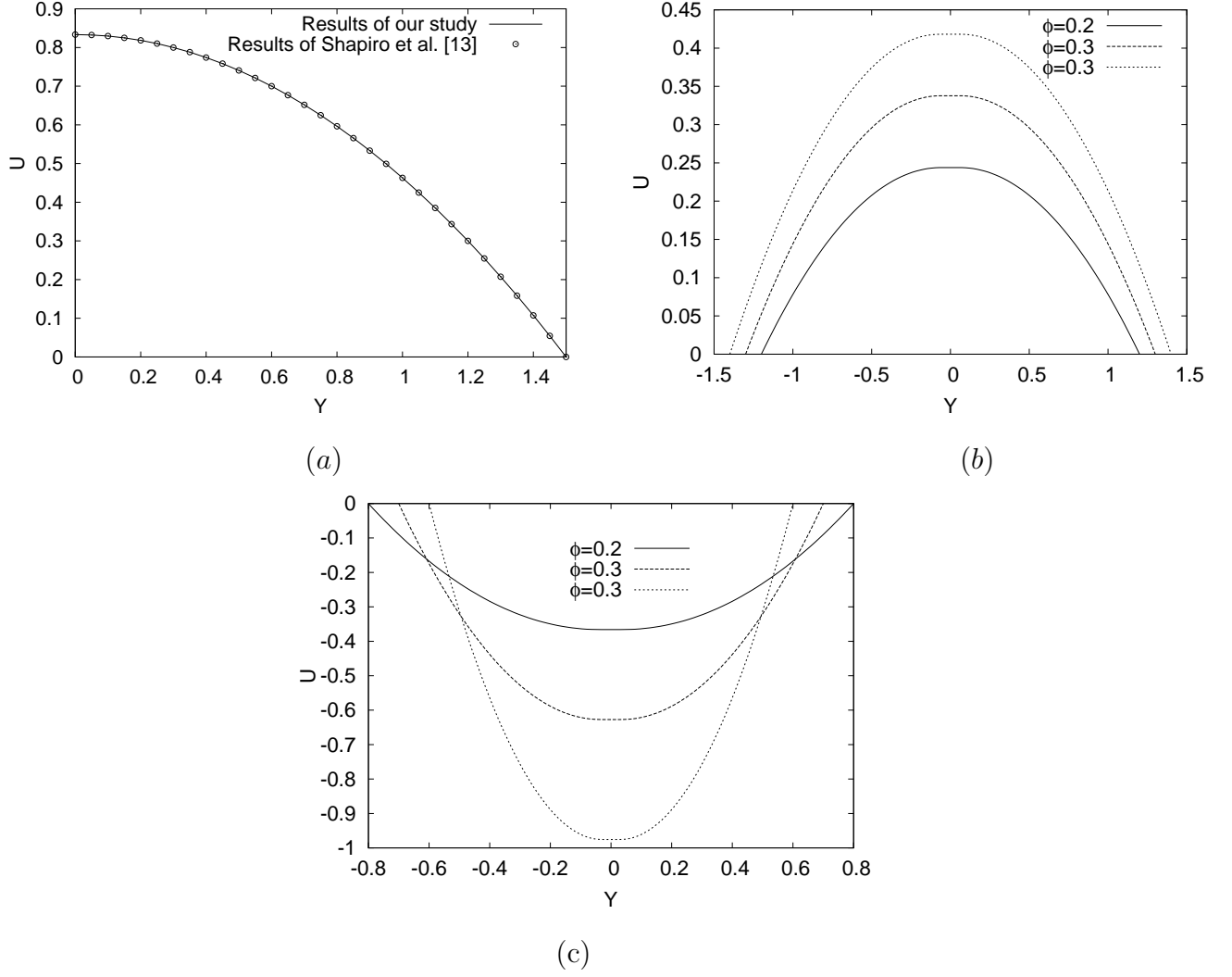
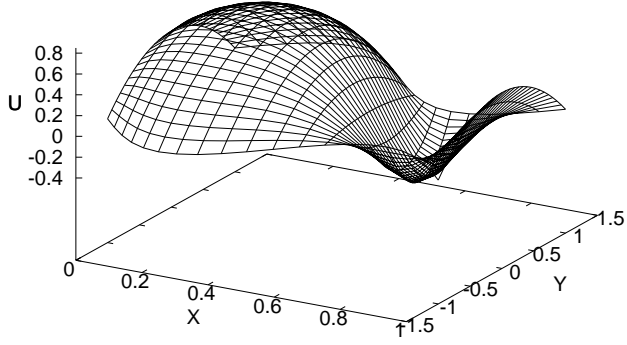
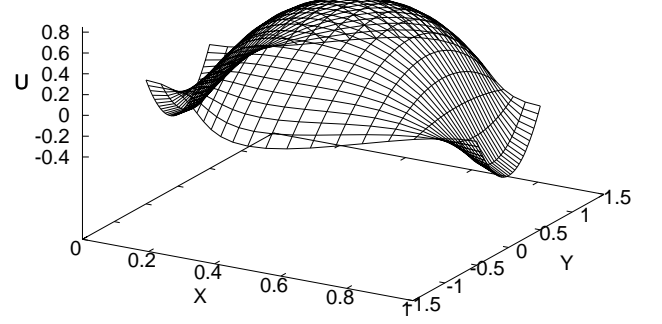


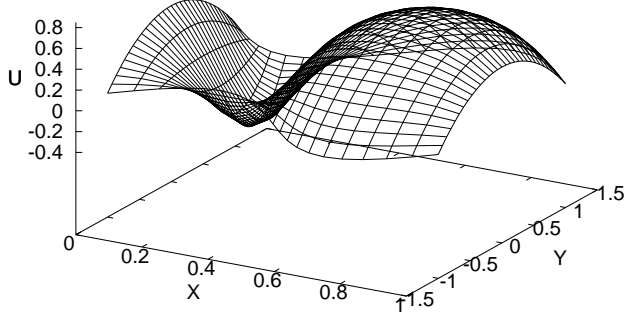
Figure 2: Variation of axial velocity in the vertical direction (a) at $x=0.5$, $t=0.25$ ($\Lambda = 0$, $\phi = 0.5$, $\tau = 0$, $n = 1$, $\Delta P = 0$) (b) for different values of ϕ at wave crest when $\Lambda = 0$, $n = 1$, $\tau = 0$, $Q = 0$ (c) for different values of ϕ at wave trough when $\Lambda = 0$, $n = 1$, $\tau = 0$, $Q = 0$



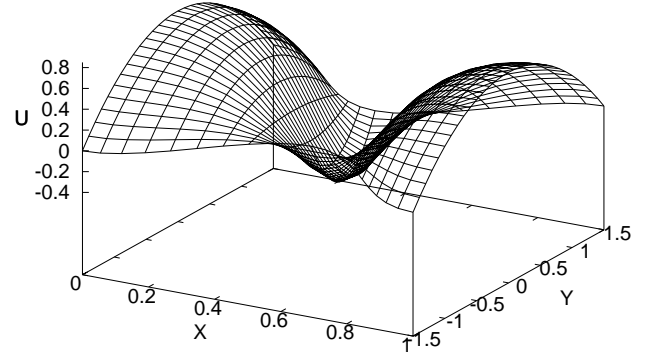
(a) for $t = 0.0$



(b) for $t = 0.25$



(c) for $t = 0.5$



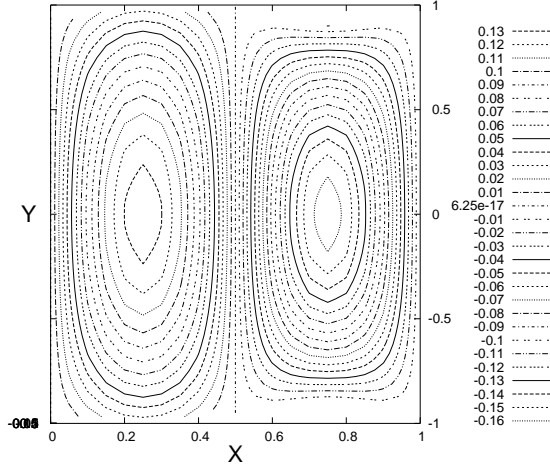
(d) for $t = 0.75$

Figure 3: Aerial view of the velocity distribution at different instants of time ($n = 1$, $\Lambda = 0$, $\Delta P = 0$, $\tau = 0$, $\phi = 0.5$)

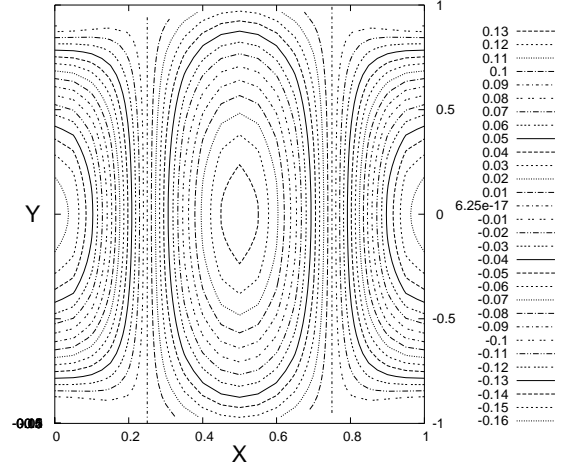
Figs. 4. The velocity contours presented in Fig. 4(b) resemble with those in Fig. 4(e) reported by Selvarajan et al. [57], although in our plots, there is a slight increase in area of contour lines at the region of wave expansion. This is possibly because the curved boundary was not taken into consideration in [57] for calculating the velocity contours.

Fig 5 gives the velocity distribution in the plane of the channel. This figure reveals that at any instant of time, although there exists a retrograde flow region, the forward flow region is predominant, the time averaged flow rate being positive. We have also found that if $Q = 0$, the retrograde flow region occupies exactly half of the one complete wave length, the remaining half being occupied by the forward mean flow region. For $t = T/4$, our study reveals that there exists two stagnation points on the axis, one being located near the trailing end and the other near the leading end. Both these observations agree with those of Takabatake and Ayukawa [27], who performed a similar study numerically for a Newtonian fluid. Fig. 6(a) shows that when $n = 1$ (that is, in the case of a Newtonian fluid) and $\Delta P = 0$, in both the forward flow region and the backward flow region velocity increases as the value of ϕ is raised. One can also have an idea of the extent by which the value of ϕ affects the axial velocity for shear thinning (cf. Fig. 6(b)) and shear thickening fluids (Fig. 6(c)). It is apparent from these figures that in either region, as τ increases, the magnitude of velocity decreases for both types of fluids.

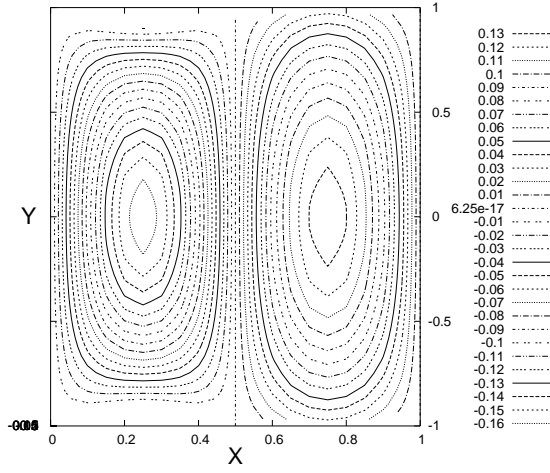
The extent to which the velocity distribution is influenced by the value of the rheological fluid index 'n' can be observed from Figs. 6(d-i) for uniform/non-uniform channels. We observe that the the parabolic nature of the velocity profiles is disturbed due to non-Newtonian effect and that as the value of 'n' increases, the magnitude of the velocity increases. It is worthwhile to mention that for a converging channel, the magnitude of the velocity is greater than that in the case of a uniform channel; however, for a diverging channel, we have an altogether different observation. Figs. 6(j-l) depict the influence of pressure on velocity distribution for shear thinning ($n < 1$)/shear thickening ($n > 1$) fluids. While the plots given in Figs. 2-6(i) correspond to the case of $\Delta P = 0$ (free pumping), Figs. 6(j-l) have been plotted for the co-pumping case $\Delta P < 0$. For these plots, we consider the case when $\Delta P = -1$. In this case, for a shear thinning fluid, flow reversal is totally absent in the case of a uniform/diverging channel. For a converging channel, however, although there is reduction in the region of flow reversal, it does not vanish altogether, irrespective of whether the fluid is of shear thinning or of shear thickening type.



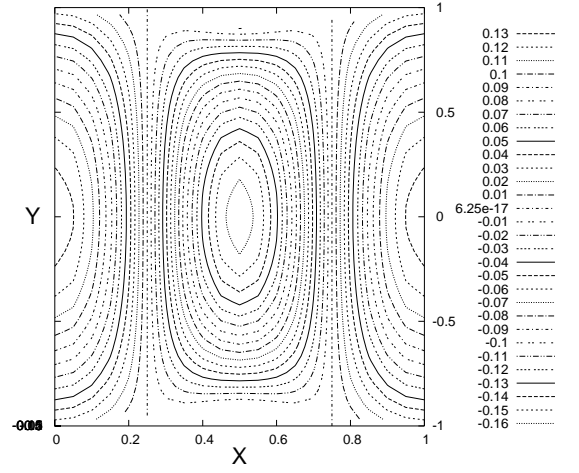
(a) for $t = 0.0$



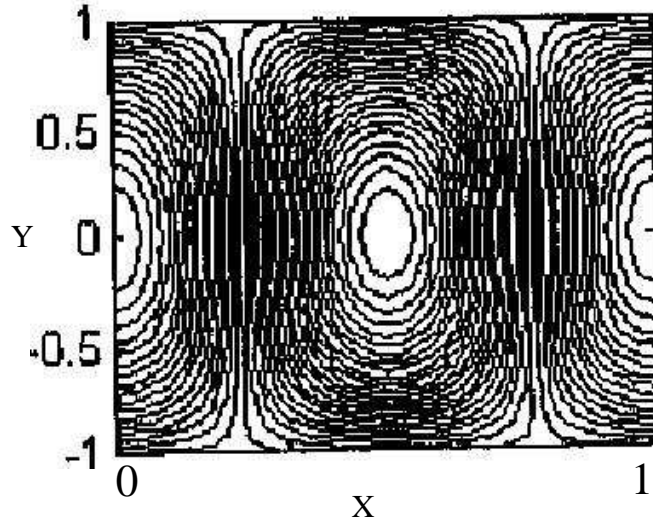
(b) for $t = 0.25$



(c) for $t = 0.5$



(d) for $t = 0.75$



(e) Contours reproduced from Selvarajan et al. [55]

Figure 4: Axial velocity contour at different time when $\phi = 0.1$, $n = 1$, $\Lambda = 0$, $\tau = 0$, $Q = 0$

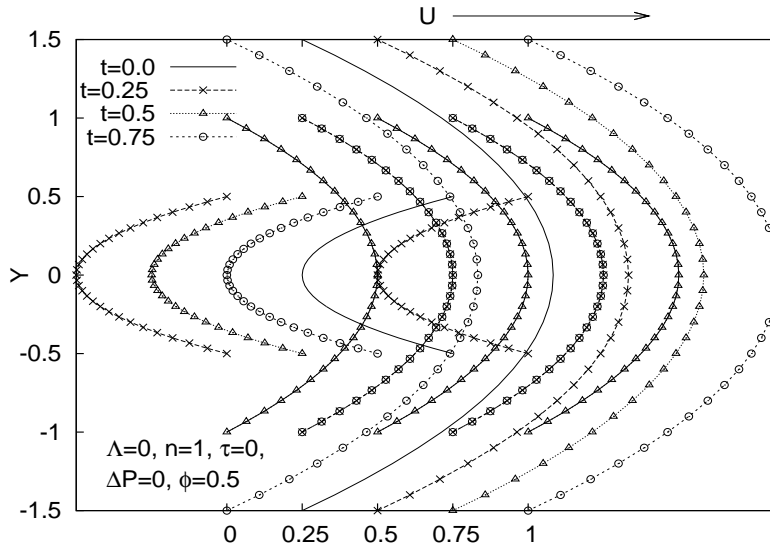
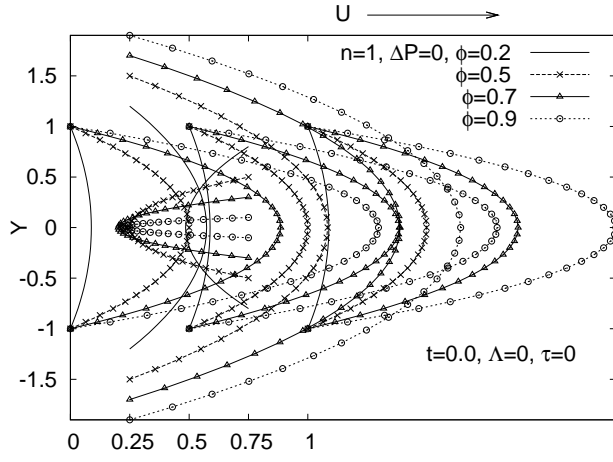


Figure 5: Velocity distribution at different instants of time

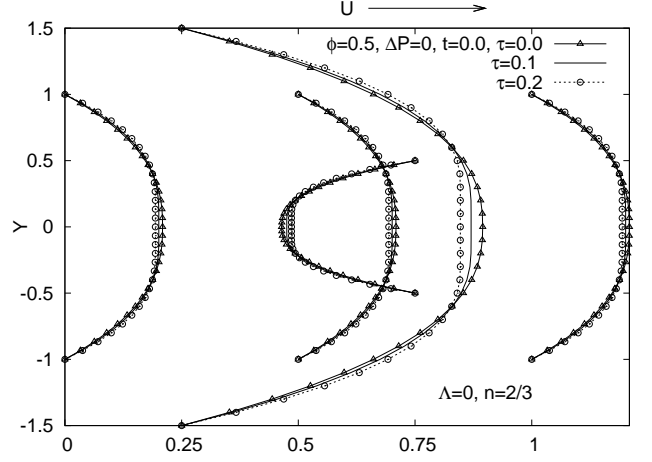
3.2 Pumping Performance

Since peristaltic transport of a fluid is associated with the concept of mechanical pumping, it is worthwhile to examine the pumping performance under the purview of the present study. The average pumping flow rate corresponding to a given pressure against which the pumping action takes place gives a measure of peristaltic pumping performance. By using lubrication theory, it has been observed by Shapiro et al. [15] that in the infinite tube model, the flow rate averaged over one wave varies linearly with pressure difference. However, the existence of a peripheral layer (Newtonian fluid), makes the relationship non-linear [58]. The present study being concerned with the peristaltic transport of a non-Newtonian fluid, the relationship between the pressure difference and the mean flow rate is found to be non-linear (cf. Figs 7(b-h)), although the study is based upon the consideration that the channel length is an integral multiple of the wave length. This has been the observation both for converging and diverging channels for all values of the fluid index n ($\neq 1$). In the Newtonian case, however, the relation is linear (cf. 7(a)) and this is in conformity to the observation reported by previous investigators [27, 59].

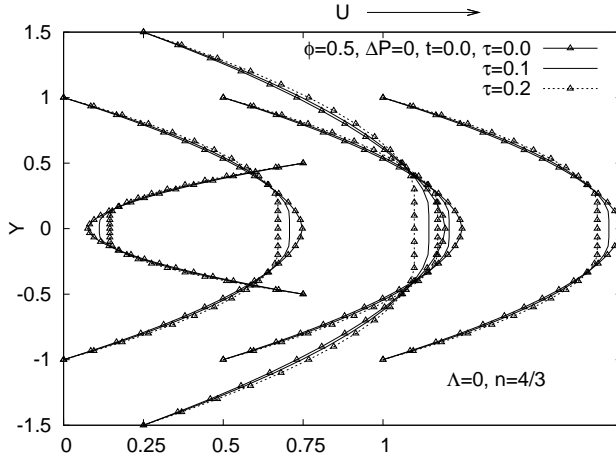
The plots in Figs. 7 show that the mean flow rate, Q increases as ΔP decreases. Figs. 7(b) and 7(c) reveal that the pumping region increases with the increase in the value of the amplitude ratio ϕ for both shear thinning and shear thickening fluids. Figs. 7(d-f) depict the influence



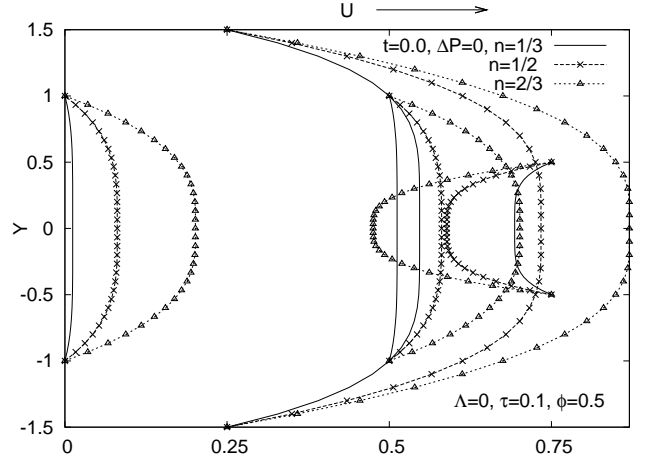
(a)



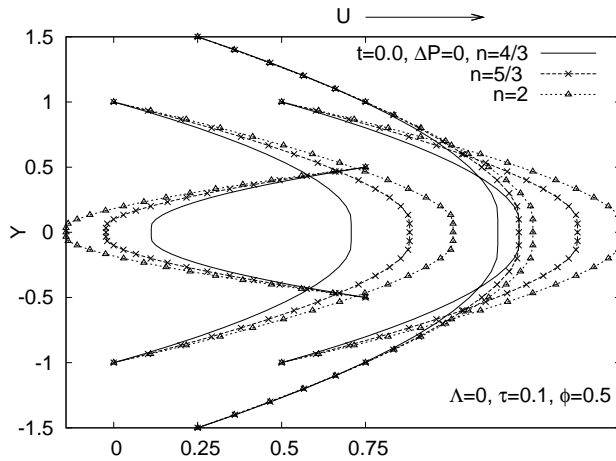
(b)



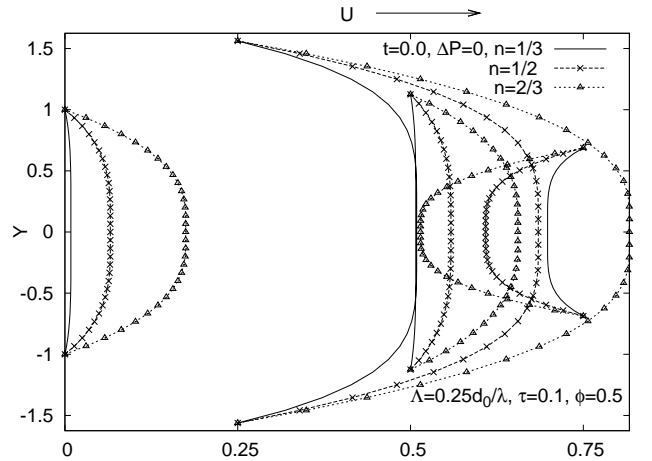
(c)



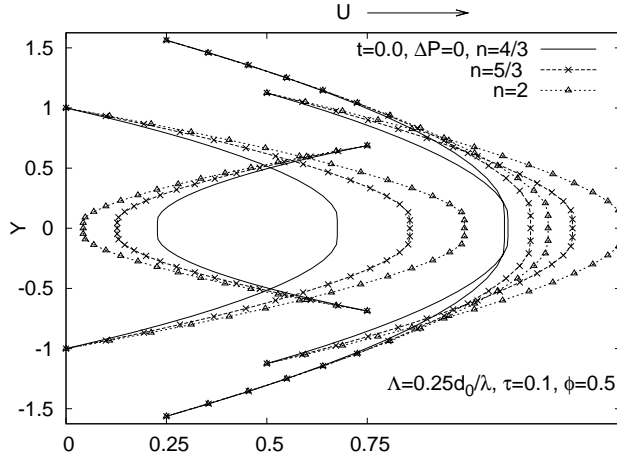
(d)



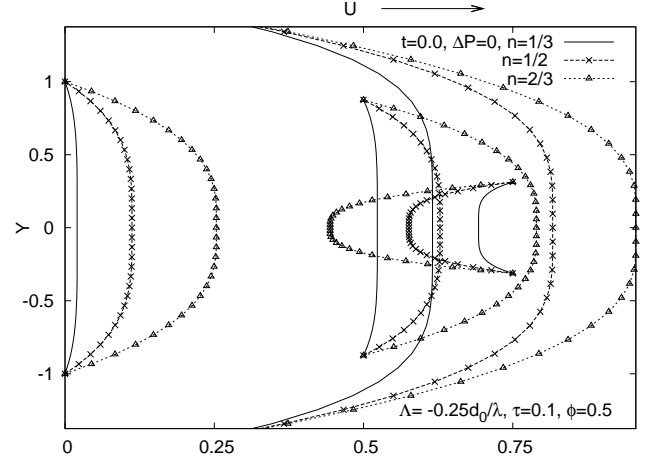
(e)



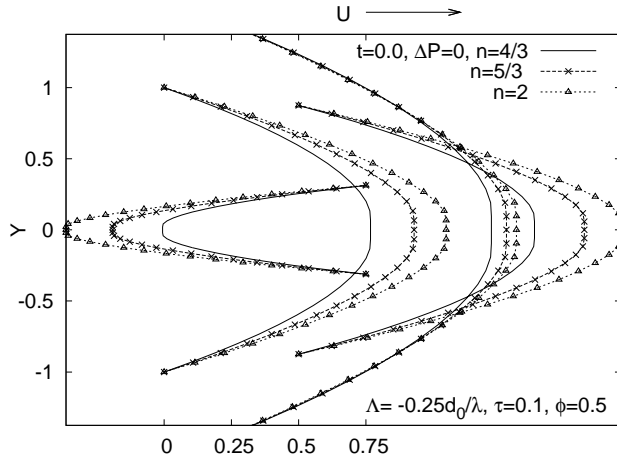
(f)



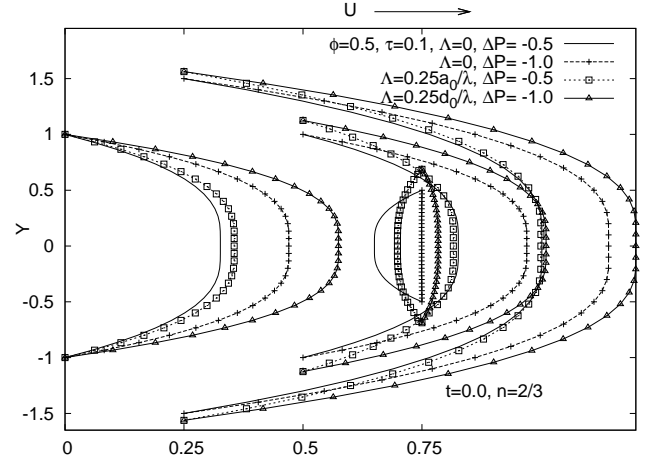
(g)



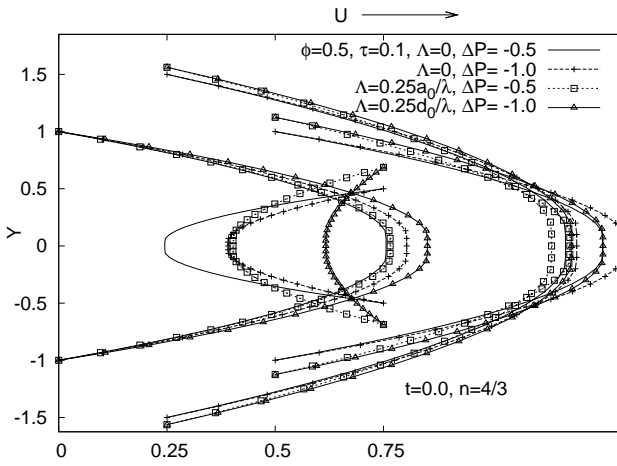
(h)



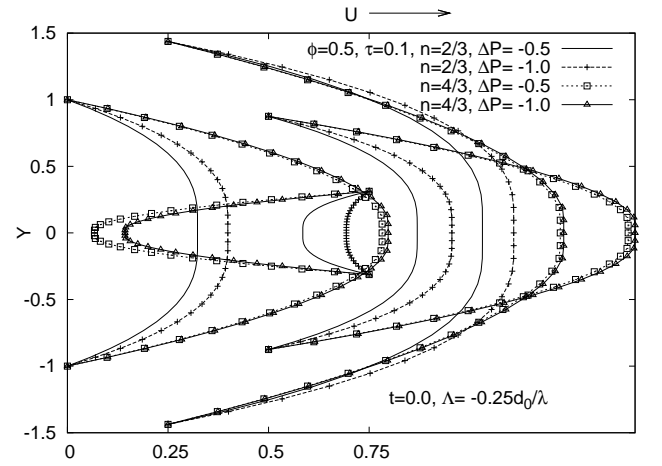
(i)



(j)

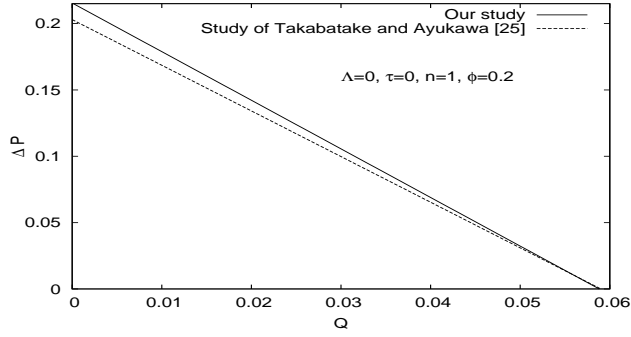


(k)

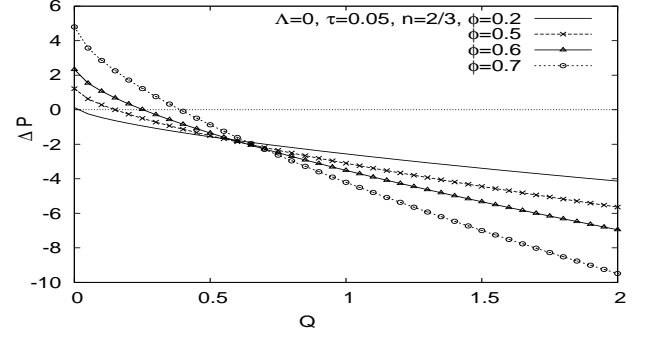


(l)

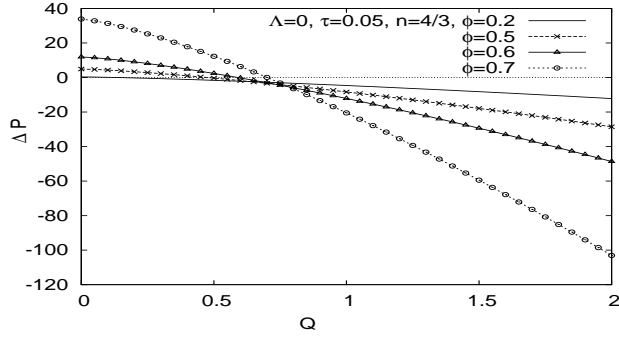
Figure 6: Distribution of velocity in different situations



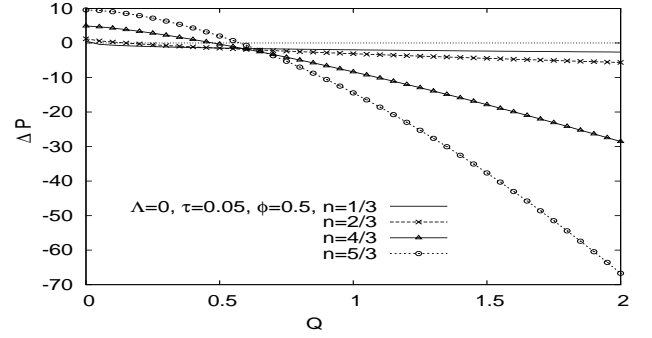
(a)



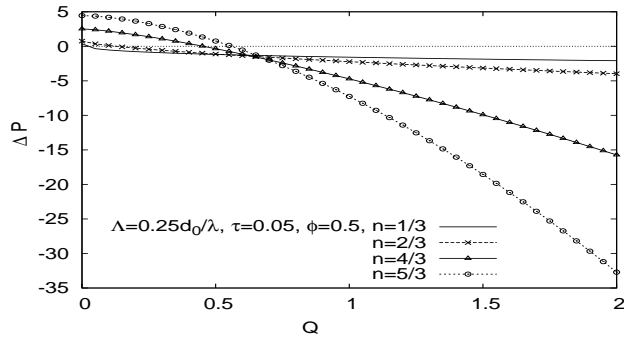
(b)



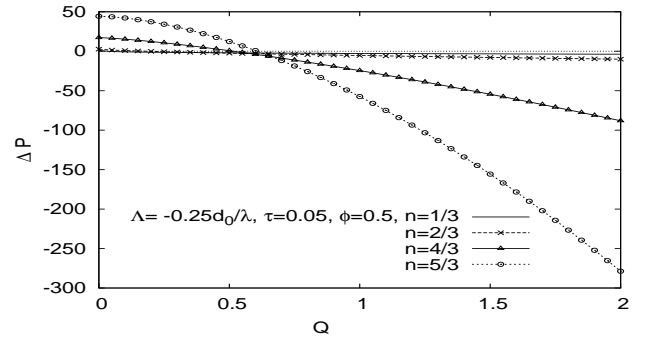
(c)



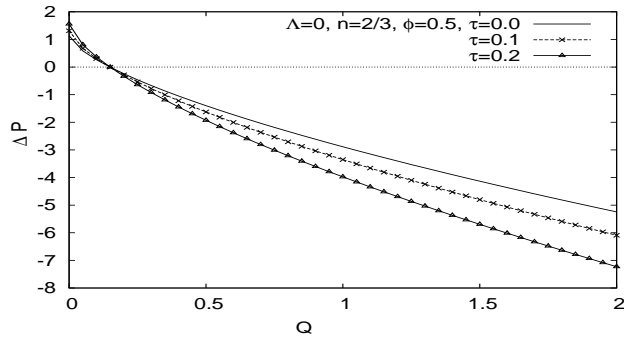
(d)



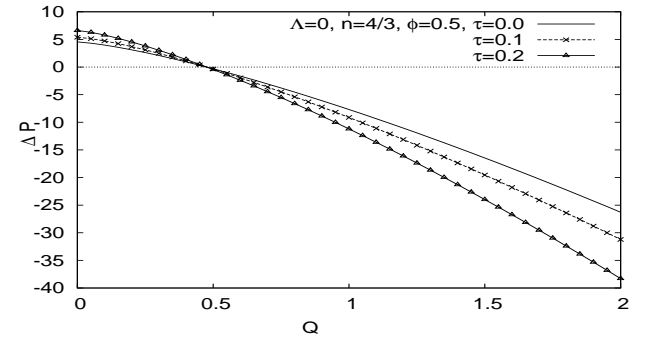
(e)



(f)



(g)



(h)

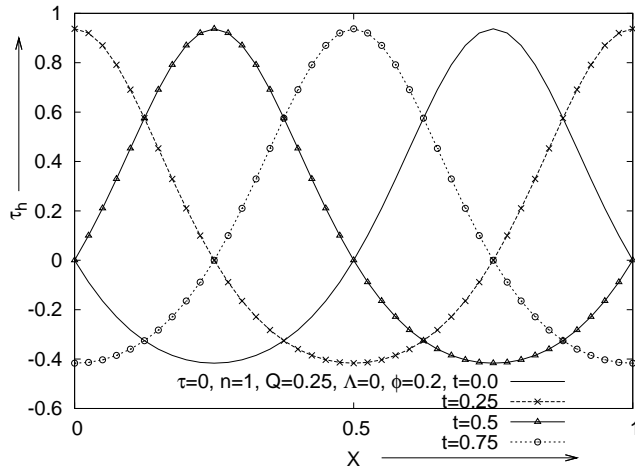
Figure 7: Pressure rise versus flow rate

of the rheological parameter ‘ n ’ on the pumping performance in uniform/diverging/converging channels. It is important to note that for all types of channels, the pumping region ($\Delta P > 0$) significantly increases with the increase in the value of ‘ n ’. In the co-pumping region ($\Delta P < 0$) the pressure rise decreases when Q exceeds a certain value. From Figs. 7(g) and 7(h), we find that Q is not significantly affected by τ for free pumping case. Moreover, when Q exceeds a certain critical limit (equal to the value of Q in the free pumping case), pressure rise decreases with the increase in τ . We further find that for both shear thinning and shear thickening fluids, pumping region increases with τ increasing; however, the effect of τ is greater in the case of shear thickening fluids.

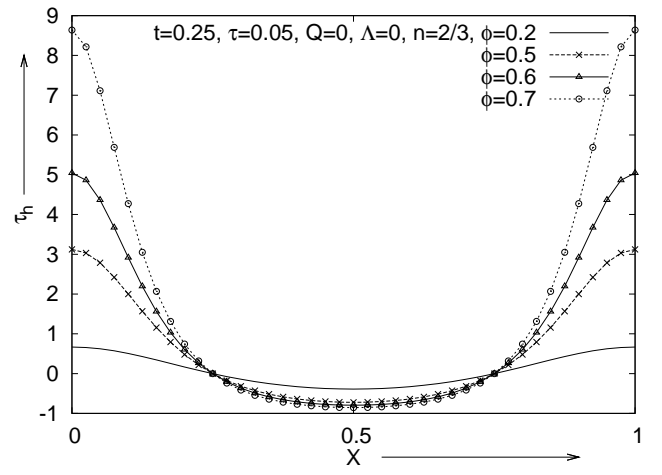
3.3 Wall Shear Stress

It is known that when the shear stress generated on the wall of a blood vessel exceeds a certain limit, there is a possibility that it can cause damage to the constituents of blood. Moreover, the magnitude of wall shear stress plays an important role in the molecular convective process at high Prandtl number/Schmidt number [60]. Because of this reason, investigation of shearing stress deserves special attention in the hemodynamical flow of blood in arteries. Figs. 8 depict the wall shear stress distribution under varied conditions. Fig. 8(a) gives the distribution of wall shear stress at four specially chosen instants of time during one complete wave period. This figure shows that at each of these time instants, there exist two peaks in the wall shear stress distribution, with a gradual ramp in between; however, negative peak of wall shear stress, τ_{min} is not as large as the maximum wall shear stress, τ_{max} . It may be observed that the transition from τ_{min} to τ_{max} takes place in the zone between the maximal height and the minimum height of the channel (cf. Fig. 8(a)). At the point of maximum occlusion, the wall shear stress as well as the pressure is maximum. The pressure gradient to the left of this point is positive and hence the local instantaneous flow will take place towards the left of τ_{max} . This may be responsible for a number of consequences. For example, if the rate of shear at the crest is quite high, a dissolving wavy wall will have a tendency to level out. Also, some chemical reaction between the wall material and the constituents of blood is likely to set in. Owing to the deposition of the products of the chemical reaction, wall amplitude increases at a rapid rate. This may lead to clogging of the blood vessel.

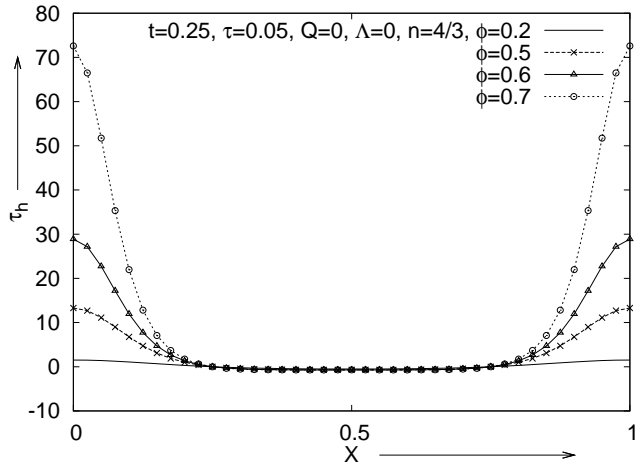
In other regions, for wall shear stress distribution curves, the peaks on both sides of τ_{max} are small. Thus the local instantaneous flow will occur in the direction of the peristaltic wave



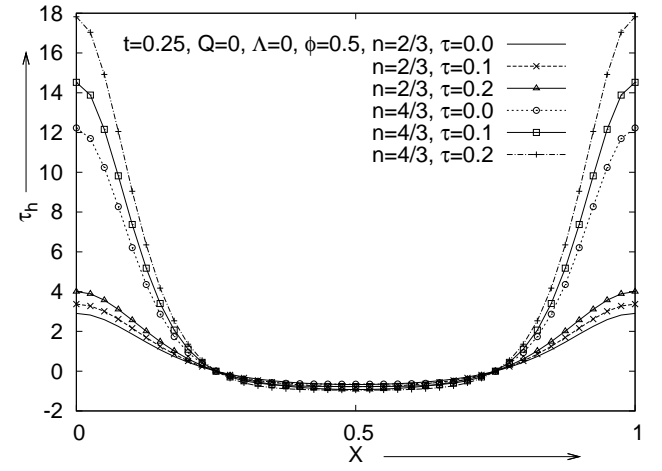
(a)



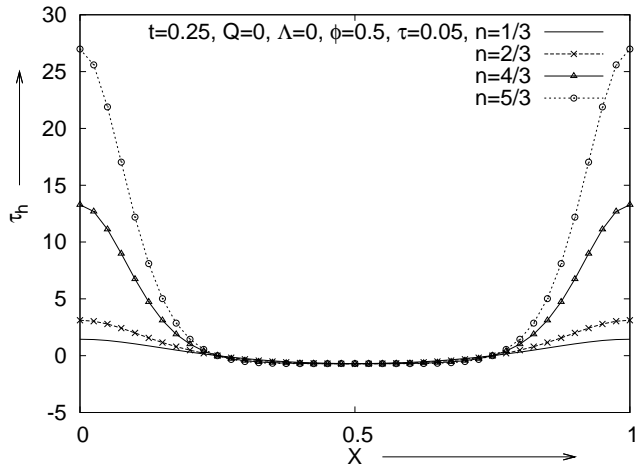
(b)



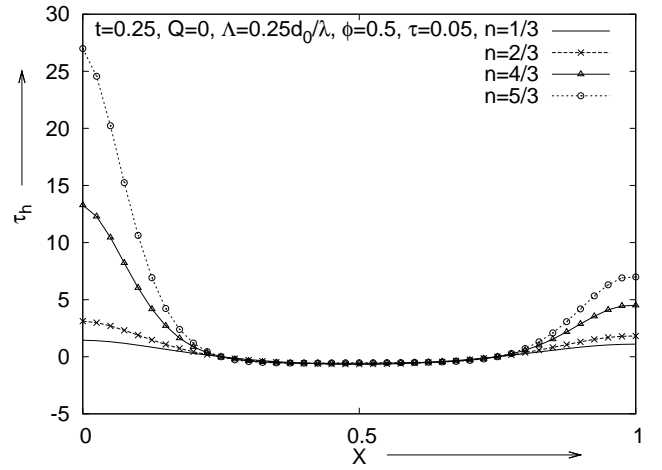
(c)



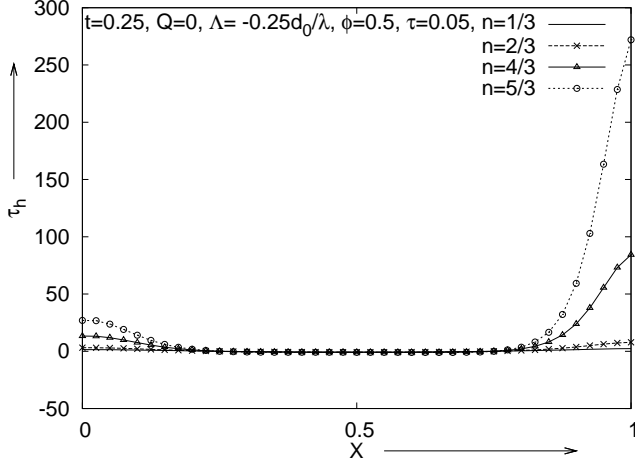
(d)



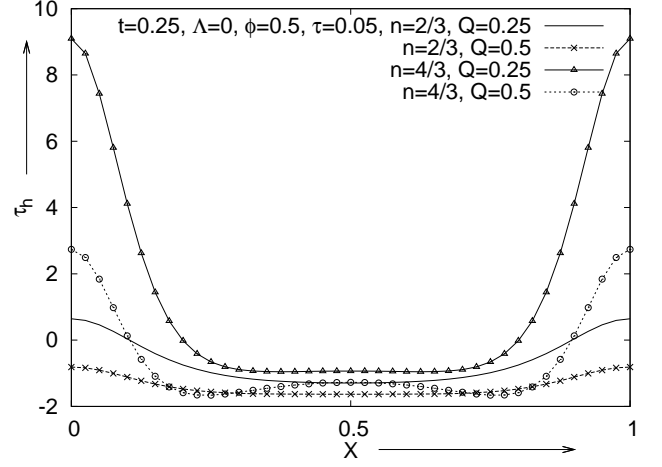
(e)



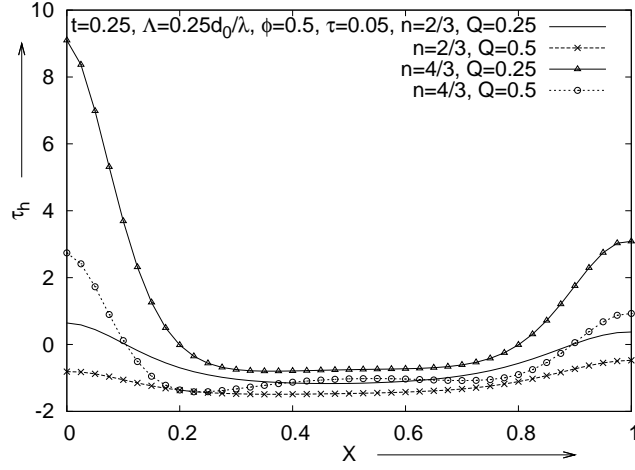
(f)



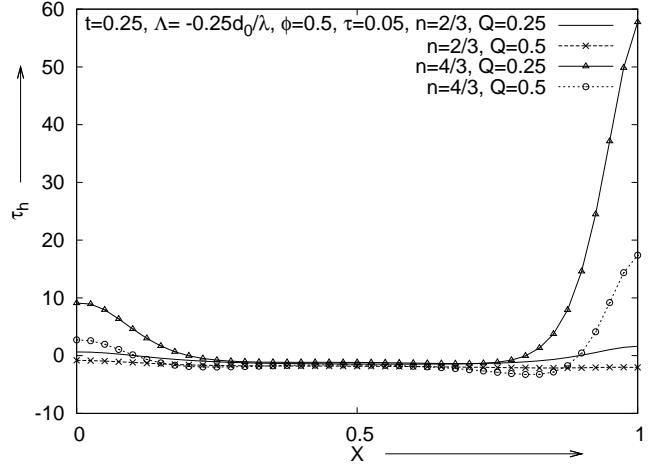
(g)



(h)

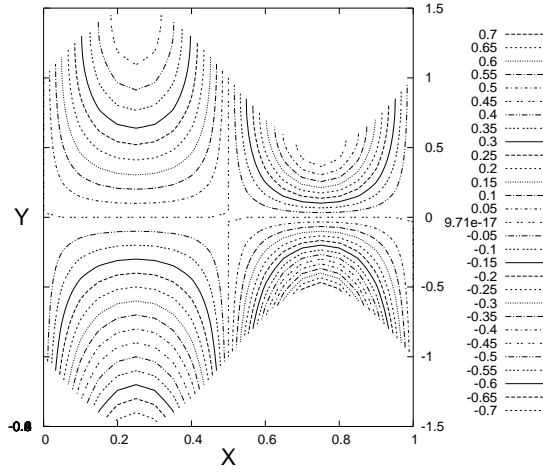


(i)

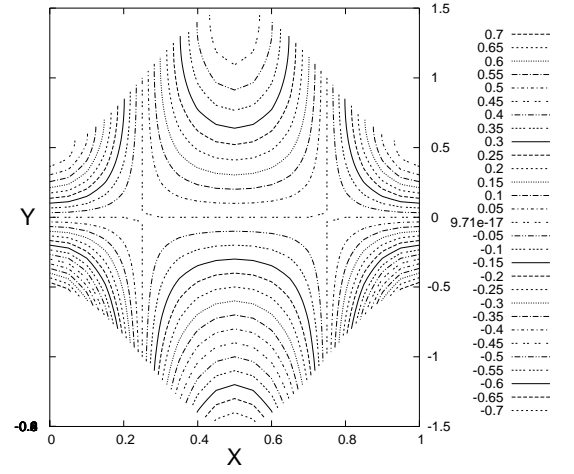


(j)

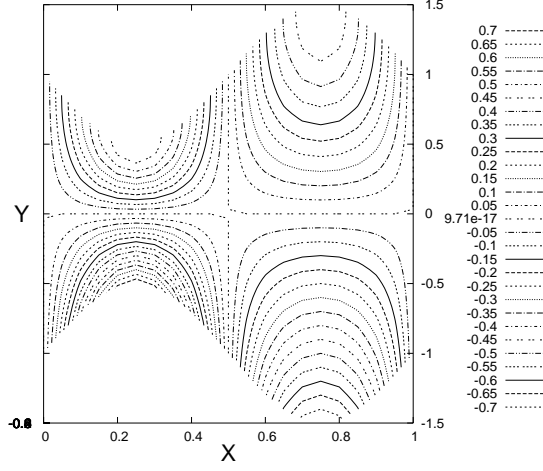
Figure 8: Wall shear stress distribution for different cases



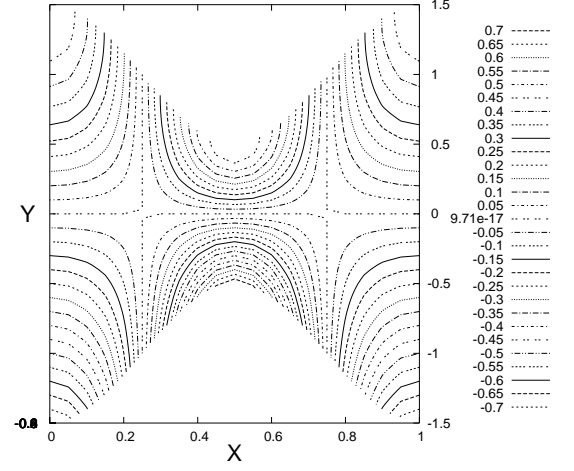
(a) for $t = 0.0$



(b) for $t = 0.25$



(c) for $t = 0.5$



(d) for $t = 0.75$

Figure 9: Streamline patterns for peristaltic flow of a Newtonian fluid at different instants of time ($Q = 0$, $\Lambda = 0$, $\tau = 0$, $\phi = 0.5$).

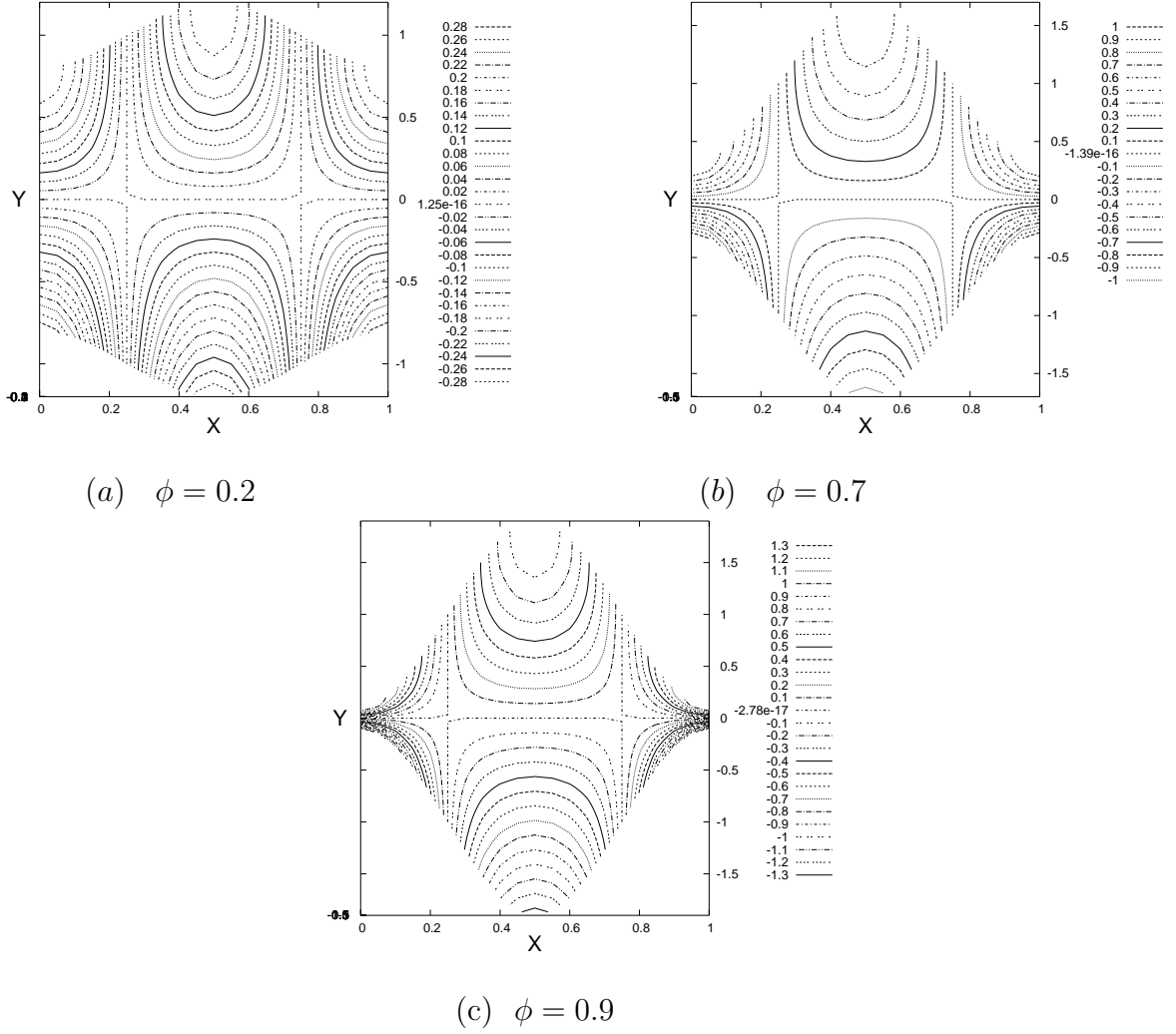


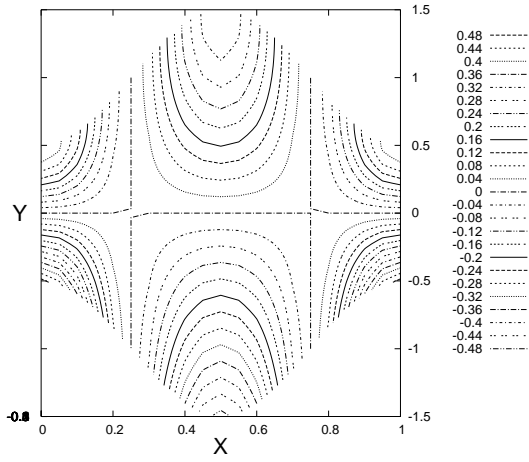
Figure 10: Streamline patterns in the case of peristaltic flow for different values of ϕ when $n = 1$, $t = 0.25$, $\tau = 0$, $\Lambda = 0$, $Q = 0$

propagation. Of course, when averaged over one wave period, net effect may be looked upon as peristaltic transport in the direction of wave propagation. It may be observed from Figs. 8(b-c) that in the contracting region where occlusion takes place, there is a significant increase in the wall shear stress due to an increase in the value of ϕ . This applies for both shear thinning and shear thickening cases. However, in the expanding region, with the increase in ϕ , τ_{min} increases in magnitude for a shear thinning fluid; for a shear thickening fluid, the effect is relatively little. Fig. 8(d) shows that τ_{max} increases with increase in τ , but for τ_{min} the effect is minimal. The effect of the rheological fluid index ‘n’ on the distribution of wall shear stress has been shown in Figs. 8(e-g) for uniform/non-uniform channels. It may be noted that in all types of channels studied here, values of τ_{max} enhance with an increase in the value of the fluid index n. Moreover, one may observe that the shear stress difference between the outlet and the inlet in the case of converging channel is exceedingly large in contrast to the case of a diverging channel. Figs. 8(h-j) indicate that as the time averaged flow rate increases, the wall shear stress decreases. This is so for all the cases examined here. It is also to be noted that the observation regarding the shear stress difference between the outlet and the inlet for $Q > 0$ is similar to that in case $Q = 0$ discussed earlier.

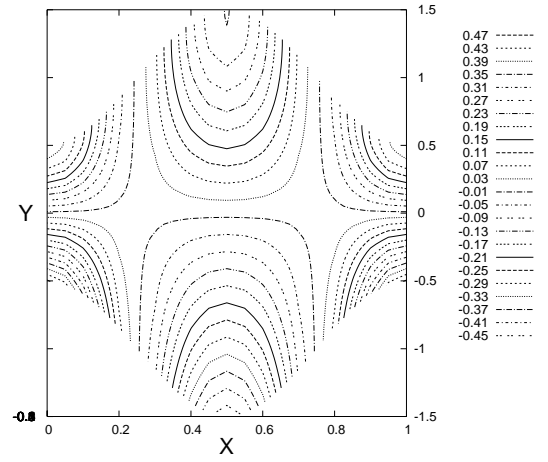
3.4 Streamlines

Figs. 9-14 gives an insight into the changes in the pattern of streamlines that occur due to changes in the values of various parameters that govern the flow of blood under the purview of the present study. Streamlines for different flow governing parameters are depicted in Figs. 9-14. These figures indicate that in the portion of the channel where it is dilating, the flow is pulled by the wall, where as in the contracting portion, the flow is pushed away from the wall. It may be noted that since the flow behaviour is unsteady in the fixed frame of reference, at different times, streamlines are of different nature. Typical nature of streamlines for the problem under the present consideration at different instants of time is shown in Figs. 9.

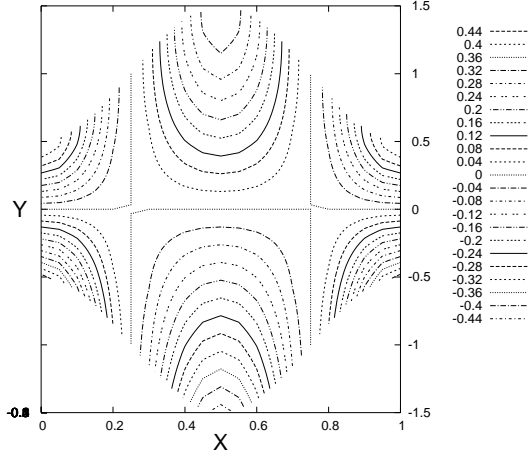
In the wave frame of reference, the formation of an internally circulating bolus of fluid that moves along with the same speed as that of the wave is a very interesting phenomenon from the view point of fluid dynamics. This physical phenomenon is usually referred to as ‘trapping’. However, in the fixed frame of reference it does not appear. It may be mentioned that investigation of the streamline patterns is quite important, particularly for some type of problems, because of the fact that the difference between the values of the stream function at any



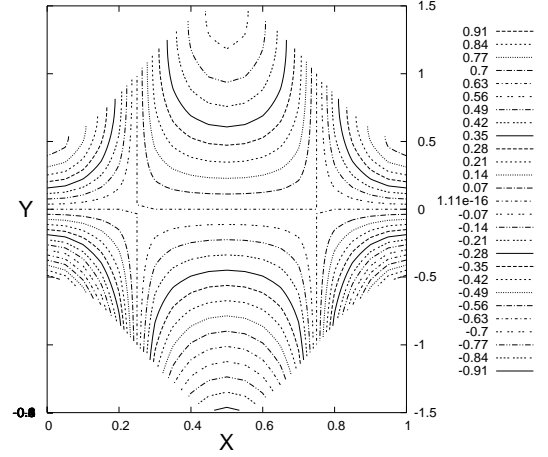
(a) $n = 2/3, \tau = 0.0$



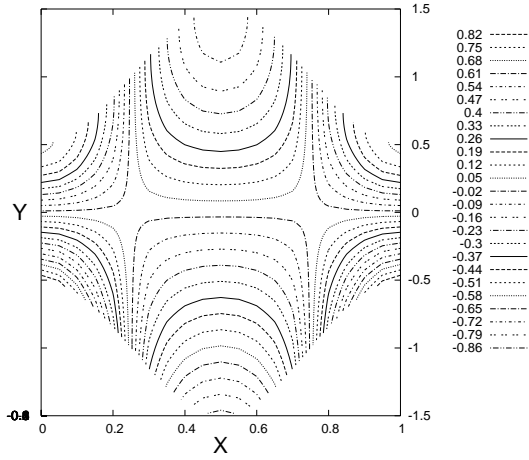
(b) $n = 2/3, \tau = 0.1$



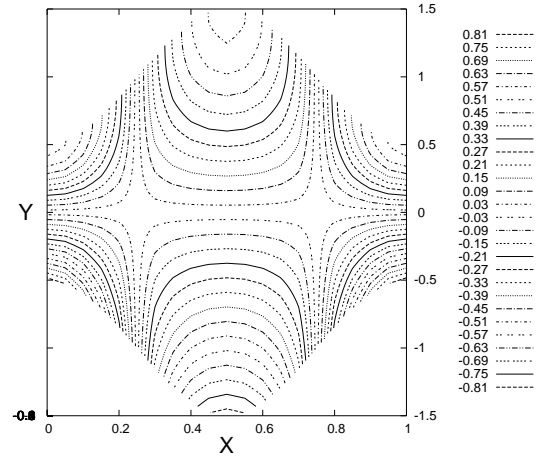
(c) $n = 2/3, \tau = 0.2$



(d) $n = 4/3, \tau = 0.0$



(e) $n = 4/3, \tau = 0.1$



(f) $n = 4/3, \tau = 0.2$

Figure 11: Streamline patterns in the case of peristaltic flow of rheological fluid for different values of τ when $Q = 0, t = 0.25, \Lambda = 0, \phi = 0.5$

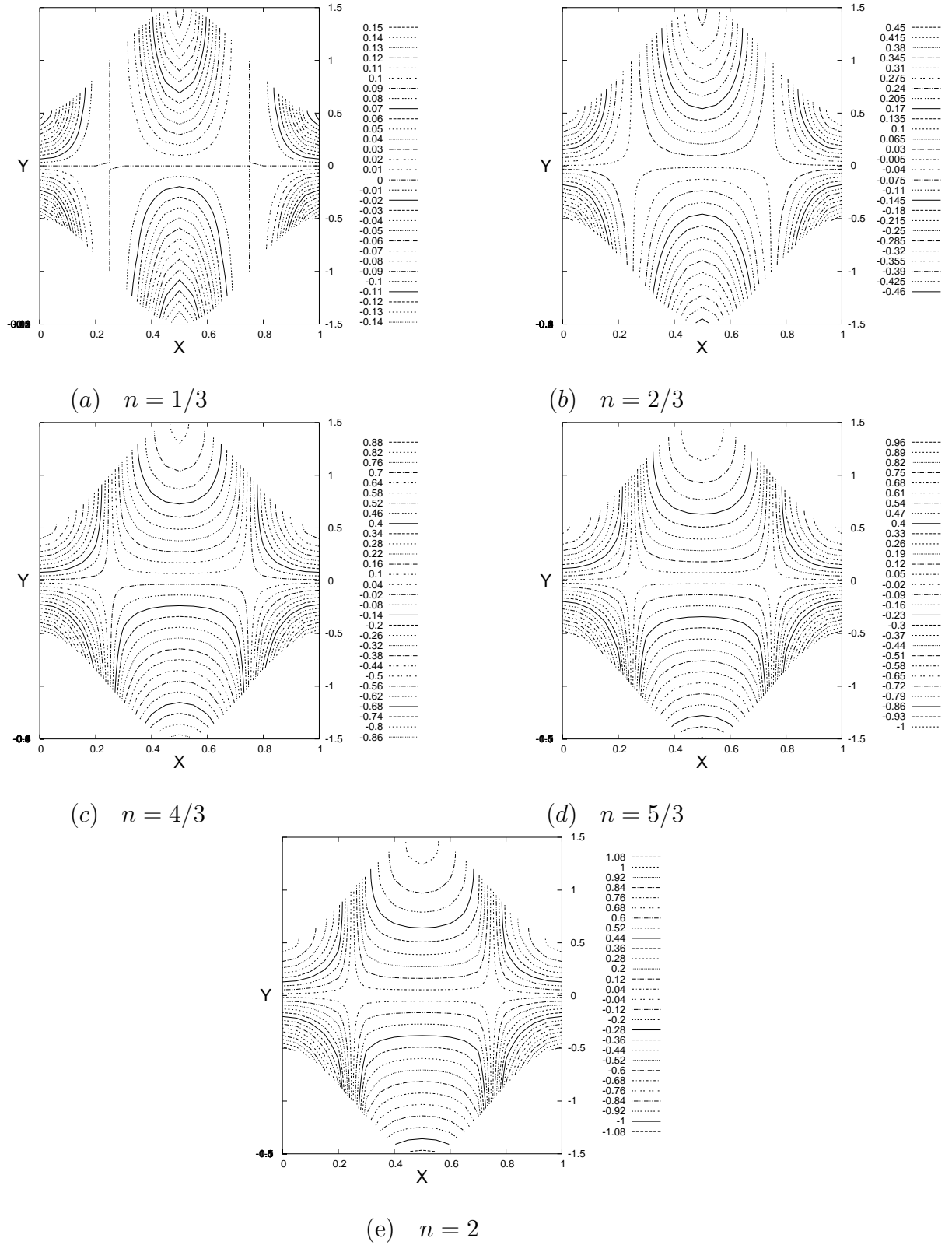


Figure 12: Streamline patterns in the case of peristaltic flow for different values of n when $Q=0$, $t=0.25$, $\tau = 0.1$, $\Lambda = 0$, $\phi = 0.5$

two points can be used to calculate the volumetric flow rate/flow flux through a line connecting the two points.

3.5 Trajectory of Particles and Reflux

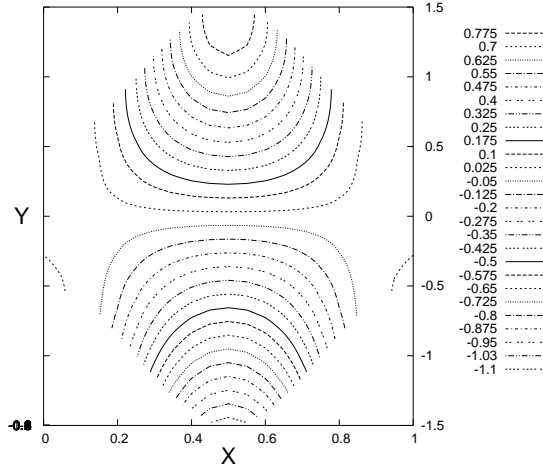
In the micro-circulatory system, the nature of trajectories of fluid particles play an important role in the functioning of arterioles. The reason is that bio-chemical reactions that take place between blood and the vessel constituents are effected by convective transport of the fluid particles. Owing to the said bio-chemical reactions there may be a fast increase in the wall amplitude. This may lead to clogging of blood. From the plots of the velocity distribution (cf. Fig. 5) it is clear that at a given cross-section, flow of blood takes place alternately in/opposite to the direction of wave propagation in different phases. The functioning of arterioles may then be affected by the confluence of the convective transport in the longitudinal direction. By investigating the pathlines of massless particles moving in the direction opposite to that of the peristaltic wave propagation in the Lagrangian frame of reference, it is possible to have an insight into the reflux phenomenon.

By resorting to appropriate numerical methods for solving the simultaneous differential equations

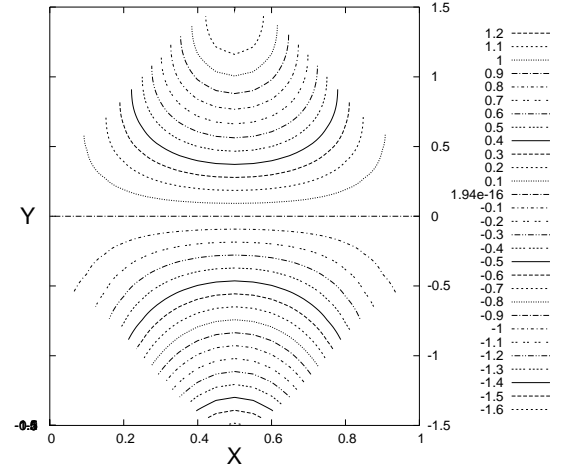
$$\frac{dX}{dt} = U, \quad \frac{dY}{dt} = V \quad (25)$$

successively starting from the initial location of the particles, it has been possible to determine the trajectories of the particles. In the above equations, (X,Y) are the non-dimensional coordinates of a particle at time t.

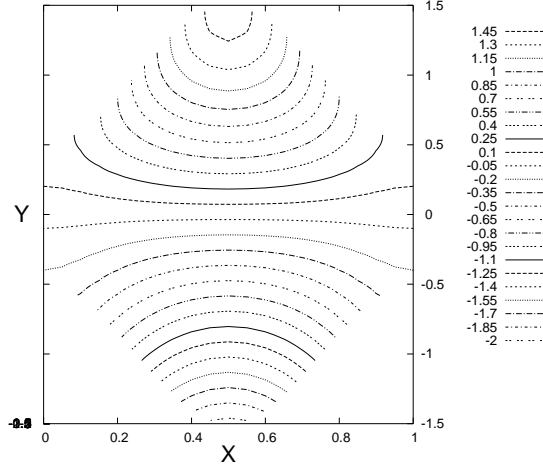
One of the novel features of this study is the examination of the particle trajectories for a non-Newtonian fluid. To the best of our knowledge and observation, no previous investigator has ever studied the trajectories for a non-Newtonian fluid. It is very important to observe that the convergence of the pathlines is very sensitive even to a moderate deviation from $n=1$. Integration of the above-written differential equations has been carried out by applying the Runge-Kutta 4 method. Figs. 15(a-b) present the trajectories for the Newtonian case, while Figs. 15(c-d) show the trajectories for the non-Newtonian case. The trajectories displayed in Fig. 15(a) are exactly similar to those reported in [15]. It is worthwhile to observe that the period of the particle is different from the wave period and that when $Q = 0$, particles in the vicinity of the axis of the channel in most cases undergo a net positive displacement, whereas



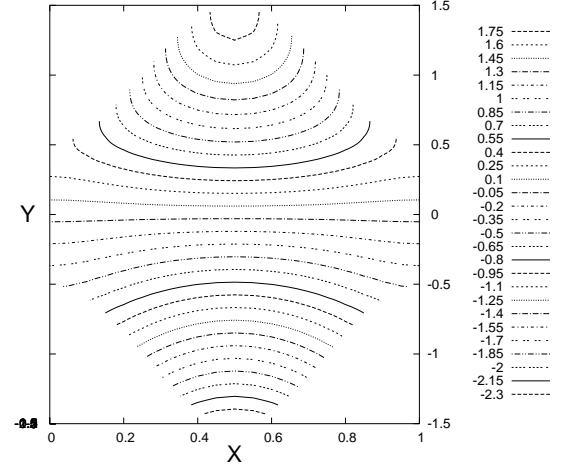
(a) for $Q = 0.25$



(b) for $Q = 0.5$

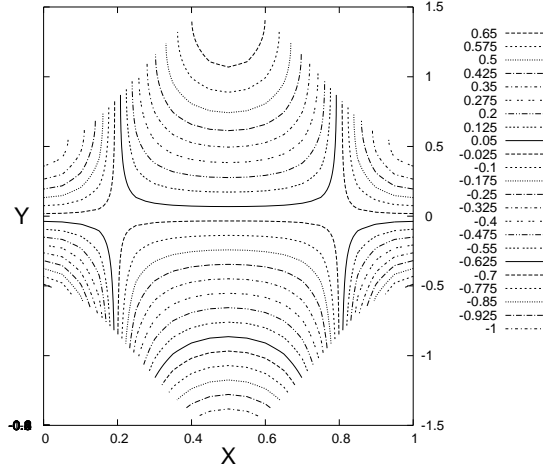


(c) for $Q = 0.75$

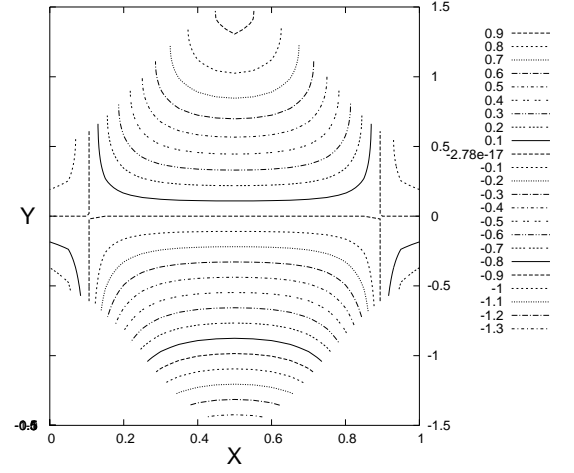


(d) for $Q = 1.0$

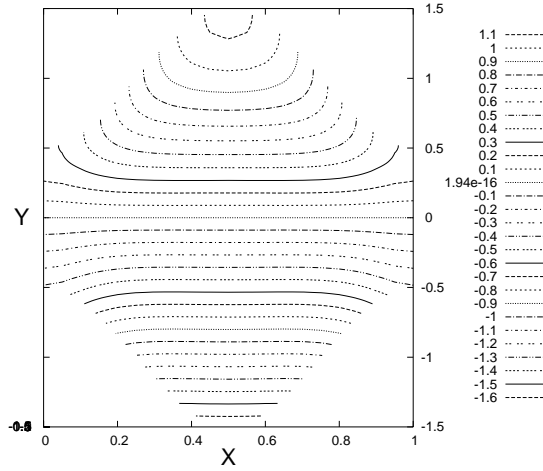
Figure 13: Streamline patterns for the peristaltic flow of a shear thinning fluid ($n=2/3$) for different values of Q when $t=0.25$, $\tau = 0.1$, $\Lambda = 0$, $\phi = 0.5$



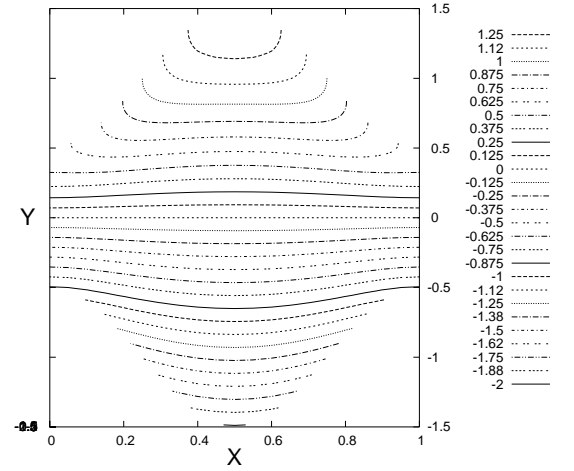
(a) for $Q = 0.25$



(b) for $Q = 0.5$



(c) for $Q = 0.75$



(d) for $Q = 1.0$

Figure 14: Streamline patterns for the peristaltic flow of a shear thickening fluid ($n=4/3$) for different values of Q when $t=0.25$, $\tau = 0.1$, $\Lambda = 0$, $\phi = 0.5$

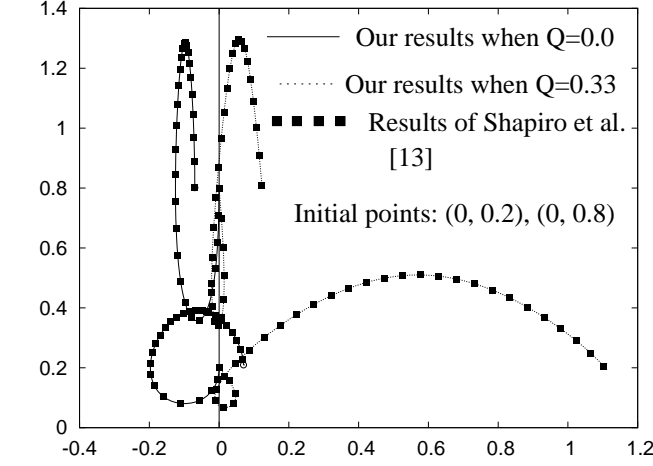
displacement of particles in the neighbourhood of the boundary is negative. These observations tally with those reported in [15, 27]. However, at the point (0.75,0.2) where the velocity profile of the particle at $x=0.75$ and time $t=0.0$ is minimum, the particle experiences a negative axial displacement (cf. Fig. 15(b)). Previous authors ([27]) also reported that even for Reynolds number 10, at certain points near the axis, the longitudinal displacement of the fluid particle can be negative. Fig. 15(c) shows that the particle period is nearly equal to the peristaltic wave period for a shear thinning fluid with $n = 2/3$. A comparison of Fig. 15(d) with Fig. 15(c) and Fig. 15(b) reveals that within one wave period, in the case of a shear thickening fluid, a fluid particle traverses more distance than in the case of a shear thinning/Newtonian fluid.

4 Validation of the Results

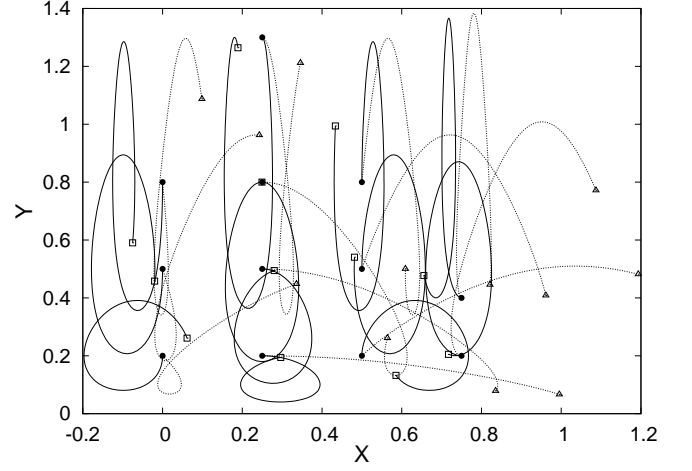
The last paragraph of Sec. 2 serves a validation of the analytical expressions derived in the present analysis. In order to validate the numerical results of the present study, we have compared our numerical results with those reported earlier by Takabatake and Ayukawa [27] on the basis of their numerical study of two-dimensional peristaltic flows. The comparison given in Fig. 7(a) shows that our results are in good agreement with those given in [27]. More particularly, one may observe from Table 1 that our results presented in Figs. 2(b,c) for the axial velocity of blood in peristaltic movement match well with the corresponding results reported in [27]. Also, a comparison between Figs. 4(b) and 4(e) shows that our results for the velocity contour are similar to those presented earlier by Selvarajan et al. [57]. Moreover, as shown in Figs. 2(a) the axial velocity variation in our case is in perfect matching with that reported by Shapiro et al. [15]. Lastly, our results presented in Fig. 15(a) are in excellent agreement with those reported in [15].

5 Summary and Conclusion

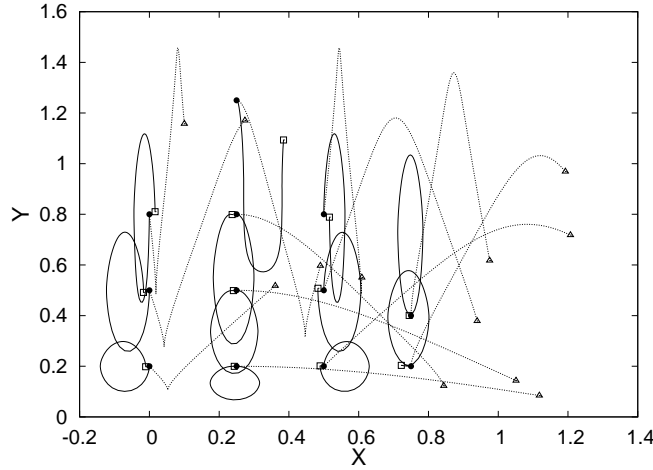
In this study, an attempt has been made to investigate the peristaltic motion of blood in the micro-circulatory system, by taking into account the non-uniform geometry of the arterioles and venules. Treating blood as a Herschel-Bulkley fluid, the effect of amplitude ratio, mean pressure gradient, yield stress and the rheological fluid index n on distribution of the velocity and wall shear stress, pumping phenomena, streamline patterns and pathlines are examined under the purview of the lubrication theory. The salient observations are as follows:



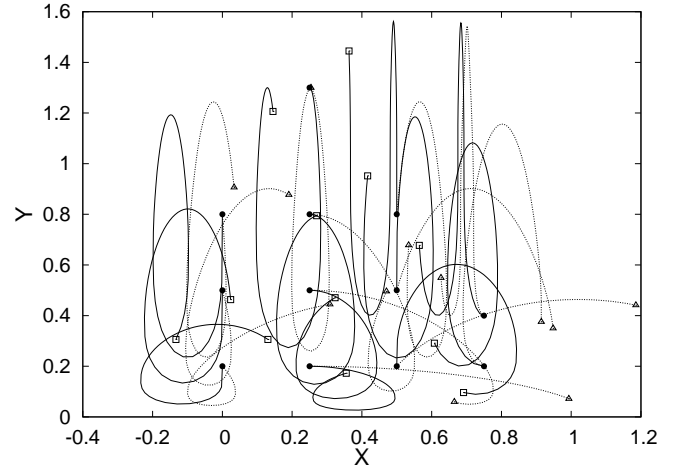
(a) for $n = 1$: comparison with [13]



(b) for $n = 1$



(c) for $n = 2/3$



(d) for $n = 4/3$

Figure 15: Trajectories of massless particles for Newtonian/non-Newtonian fluids at different locations ($Q = 0$, $\phi = 0.5$, $\tau = 0$, $\Lambda = 0$); — for $Q=0$; \cdots for $Q = 3\phi^2/(2 + \phi^2)$; \bullet initial locations; \square at the end of one wave period if $Q = 0$; \triangle at the end of one wave period if $Q = 3\phi^2/(2 + \phi^2)$; \circ at the end of one particle period if $Q=0$; $*$ at the end of one particle period if $Q = 3\phi^2/(2 + \phi^2)$. In Fig. (a) \blacksquare stand for the corresponding results reported by Shapiro et al. [13]

(i) At any instant of time, there is a retrograde flow region for both Newtonian and non-Newtonian fluids, when $\Delta P = 0$ and also for some negative values of ΔP .

(ii) With an increase in the value of n and ϕ , the regions of forward/retrograde flow advance at a faster rate.

(iii) The parabolic nature of the velocity profiles are significantly affected by the value of the rheological fluid index ' n '.

(iv) In case of a shear thinning fluid, flow reversal does not occur in the case of a channel having uniform geometry; it transforms to forward flow in the case of a diverging channel. For a shear thickening fluid, flow reversal reduces, but it does not vanish altogether when ΔP changes from 0 to -1 .

(v) Non-uniform geometry affects quite significantly the distribution of velocity and wall shear stress as well as the pumping phenomena and other flow characteristics.

(vi) Peristaltic pumping characteristics as well as the distribution of velocity and wall shear stress are strongly influenced by the amplitude ratio ϕ and the rheological fluid index ' n '.

The study bears the potential of significant application to the field of biomedical engineering and technology, because it is known that in roller pumps, the fluid elements are quite prone to significant damage of fluid elements; also, in the process of transportation of fluids in living organisms, by using arthro-pumps, the fluid particles are likely to be appreciably damaged. Moreover, the qualitative and quantitative aspects of the present investigation for the wall shear stress have a significant bearing on extra-corporeal circulation, where the heart-lung machine is usually used. In this case, there is a possibility that the erythrocytes of blood may get damaged.

Acknowledgment: *The authors wish to express their deep sense of gratitude to all the reviewers for their learned comments and suggestions based upon which the manuscript has been thoroughly revised. One of the authors (S. Maiti) is thankful to the Council of Scientific and Industrial Research (CSIR), New Delhi for their financial support towards this study.*

References

- [1] Misra J. C. and Pandey S. K. 1999. Peristaltic transport of a non-Newtonian fluid with a peripheral layer. *International Journal of Engineering Science*, 37, 1841-1858.
- [2] Misra J. C. and Pandey S. K. 2001. Peristaltic flow of a multi-layered power-law fluid through a cylindrical tube. *International Journal of Engineering Science*, 39, 387-402.

- [3] Misra J. C. and Pandey S. K. 2002. Peristaltic transport of blood in small vessels: study of a mathematical model. *Computers & Mathematics with Applications*, 4, 1183-1193.
- [4] Misra J. C. and Pandey S. K. 1994. Peristaltic transport of a particle-fluid suspension in a cylindrical tube, *Computers & Mathematics with Applications*, 28, 131-145.
- [5] Misra J. C. and Pandey S. K. 1995. Peristaltic transport in a tapered tube. *Mathematical and Computer Modelling*, 22, 137-151.
- [6] Misra J. C. and Pandey S. K. 2001. A mathematical model for oesophageal swallowing of a food-bolus. *Mathematical and Computer Modelling*, 33, 997-1009.
- [7] Misra J. C. and Pandey S. K. 2006. Peristaltic transport of physiological fluids, In Misra J. C., *Biomathematics: Modelling and Simulation*, 166-193, World Scientific, London/Singapore.
- [8] Misra J. C., Maiti S. and Shit G.C. 2008. Peristaltic Transport of a Physiological Fluid in an Asymmetric Porous Channel in the Presence of an External Magnetic Field. *Journal of Mechanics in Medicine and Biology*, 8(4), 507-525.
- [9] Misra J. C. and Maiti S. 2011. Peristaltic Transport of a Rheological Fluid: Model for Movement of Food Bolus Through Esophagus. *Applied Mathematics and Mechanics* (accepted for Publication), arXiv:1112.6076v1 [physics.flu-dyn]
- [10] Maiti S. and Misra J. C. 2011. Peristaltic Flow of a Fluid in a Porous Channel: a Study Having Relevance to Flow of Bile. *International Journal of Engineering Science*, 49, 950-966.
- [11] Maiti S. and Misra J. C. 2012. Peristaltic Transport of a Couple Stress Fluid: Some Applications to Hemodynamic. *Journal of Mechanics in Medicine and Biology*, 12(1), 1-21.
- [12] Guyton A. C. and Hall J. E. 2006. *Text Book of Medical Physiology*. Elsevier: Saunders Co.
- [13] Jaffrin M. Y. and Shapiro A. H. 1971. Peristaltic pumping. *Annual Review of Fluid Mechanics*, 3, 13-36.
- [14] Fung Y. C. and Yih C. S. 1968. Peristaltic Transport. *Journal of Applied Mechanics*, 35, 669-75.
- [15] Shapiro A. H., Jaffrin M. Y. and Weinberg, S.L. 1969. Peristaltic pumping with long wavelength at low Reynolds number. *Journal of Fluid Mechanics*, 37, 799-825.
- [16] Srivastava L. M. and Srivastava V.P. 1984. Peristaltic transport of blood: Casson model: II. *Journal of Biomechanics*, 17 821-29.
- [17] Usha S. and Rao, A. R. 2000. Effect of curvature and inertia on the peristaltic transport in a two fluid system. *International Journal of Engineering Science*, 38, 1355-75.

- [18] Mishra M. and Rao A. R. 2005. Peristaltic transport in a channel with a porous peripheral layer: model of a flow in gastrointestinal tract. *Journal of Biomechanics*, 38, 779-789.
- [19] Yaniv S., Jaffa A. J., Eytan O. and Elad D. 2009. Simulation of embryo transport in a closed uterine cavity model. *European Journal of Obstetrics Gynecology and Reproductive Biology*, 144S, S50-S60.
- [20] Jimenez-Lozano J., Sen M. and Dunn P. F. 2009. Particle motion in unsteady two-dimensional peristaltic flow with application to the ureter. *Physical Review E*, 041901.
- [21] Wang Y., Ali N., Hayat T. and Oberlack M. 2011. Peristaltic motion of a magnetohydrodynamic micropolar fluid in a tube. *Applied Mathematical Modelling*, 35(8), 3737-3750.
- [22] Hayat T., Khan M., Siddiqui A. M. and Asghar S. 2007. Non-linear peristaltic flow of a non-Newtonian fluid under effect of a magnetic field in a planar channel. *Communications in Nonlinear Science and Numerical Simulation*, 12(6), 910-919.
- [23] Misra J. C. and Chakravarty S. 1982. Dynamic response of arterial walls in vivo. *Journal of Biomechanics*, 15, 317-324.
- [24] Misra J. C. and Chakravarty S. 1986. Flow in arteries in the presence of stenosis. *Journal of Biomechanics*, 19, 907-916.
- [25] Misra J. C. and Patra M. K. 1993. A Non-Newtonian Fluid Model for Blood Flow Through Arteries Under Stenotic Conditions. *Journal of Biomechanics*, 26, 1129-1141.
- [26] Usha S. and Rao A. R. 1995. Peristaltic transport of a biofluid in a pipe of elliptic cross section. *Journal of Biomechanics*, 28(1), 45-52.
- [27] Takabatake S and Ayukawa K. 1982. Numerical study of two-dimensional peristaltic flows. *Journal of Fluid Mechanics* 122, 439-465.
- [28] Pozrikidis C. 1987. A study of peristaltic flow. *Journal of Fluid Mechanics* 80, 515-527.
- [29] Jimenez-Lozano J. and Sen M. 2010. Particle dispersion in two-dimensional peristaltic. *Physics of Fluids*, 22, 043303.
- [30] Bhargava R., Sharma S., Takhar H. S., Beg T. A., Beg O. A. and Hung T. K. 2006. Peristaltic pumping of micropolar fluid in porous channel: model for stenosed arteries. *Journal of Biomechanics*, 39 (Supplement 1), S649.
- [31] Bohme G and Friedrich R. 1983. Peristaltic transport of viscoelastic liquids. *Journal of Fluid Mechanics*, 128, 109-122.
- [32] Srivastava L. M. and Srivastava V. P. 1985. Peristaltic transport of a non-Newtonian fluid: a applications to the vas deferens and small intestine. *Annals of Biomedical Engineering* 13, 137-153.

- [33] Provost A. M. and Schwarz W. H. 1994. A theoretical study of viscous effects in peristaltic pumping. *Journal of Fluid Mechanics* 279, 177-195.
- [34] Chakraborty S. 2006. Augmentation of peristaltic micro-flows through electro-osmotic mechanisms. *Journal of Physics D: Applied Physics*, 39, 5356-5363.
- [35] Rand P. W., Lacombe E, Hunt H. E. and Austin W. H. 1964. Viscosity of normal blood under normothermic and hypothermic conditions. *Journal of Applied Physiology*, 19, 117-122.
- [36] Bugliarello G., Kapur C. and Hsiao G. 1965. The profile viscosity and other characteristics of blood flow in a non-uniform shear field. *Proc IVth International Congress on Rheology*, 4, Symp of Biorheol (Ed. Copley A L), 351-370, Interscience, New York.
- [37] Chien S., Usami S., Taylor H. M, Lundberg J. L. and Gregerson M.T. 1965. Effects of hematocrit and plasma proteins on human blood rheology at low shear rates. *Journal of Applied Physiology*, 21, 81-87.
- [38] Masud A. and Kwack J. 2011. A stabilized mixed finite element method for the incompressible shear-rate dependent non-Newtonian fluids: Variational Multiscale framework and consistent linearization. *Computer Methods in Applied Mechanics and Engineering*, 200, 577-596.
- [39] Kwack J. and Masud A. 2010. A Three-field Formulation for Incompressible Viscoelastic Fluids. *International Journal of Engineering Science*, 48, 1413-1432.
- [40] Anand C. M. and Rajagopal K. R. 2004. A shear-thinning viscoelastic fluid model for describing the flow of blood. *International Journal of Cardiovascular Medicine and Science*, 4, 59-68.
- [41] Charm S. E. and Kurland G. S. 1965. Viscometry of human blood for shear rates of 0-100,000 sec^{-1} . *Nature* 206, 617-629.
- [42] Charm S. E. and Kurland G. S. 1974. *Blood Flow and Microcirculation*. New York: John Wiley.
- [43] Merrill F. W., Benis A. M., Gilliland E. R., Sherwood T. K. and Salzman E. W. 1965. Pressure flow relations of human blood in hollow fibers at low flow rates. *J Applied Physiology*, 20, 954-967.
- [44] Blair G. W. S. and Spanner D. C. 1974. *An Introduction to Bioreheology*. Elsevier, Amsterdam.
- [45] Wiedman, M.P 1963. Dimensions of blood vessels from distributing artery to collecting vein. *Circulation Research*, 12, 375-381.
- [46] Wiederhielm C. A. 1967. Analysis of small vessel function, In *Physical Bases of Circulatory Transport: Regulation and Exchange*, edited by Reeve, E. B. and Guyton, A. C., 313-326, W. B.Saunders, Philadelphia.

- [47] Lee J. S., Fung Y. C. 1971. Flow in nonuniform small blood vessels. *Microvascular Research*, 3, 272-287.
- [48] Gupta B. B. and Seshadri V. J. 1976. Peristaltic pumping in non-uniform tubes. *Journal of Biomechanics*, 9, 105-109.
- [49] Srivastava L. M. and Srivastava V. P. 1983. Peristaltic transport of a physio-logical fluid, part I: Flow in non-uniform geometry. *Biorheology*, 20, 153-166.
- [50] Malek J., Necas J. and Rajagopal K. R. 2002. Global existence of solutions for fluids with pressure and shear dependent viscosities. *Applied Mathematics Letters* 15, 961-967.
- [51] Huang X. and Garcia H. A. 1998. Herschel-Bulkley model for mud flow down a slope. *Journal of Fluid Mechanics*, 374, 305-333.
- [52] Lardner T. J. and Shack W. J. 1972. Cilia transport. *Bulletin of Mathematical Biology*, 34, 325-335.
- [53] Barbee K. A, Davies P. F. and Lal R. 1994. Shear stress-induced reorganization of the surface topography of living endothelial cells imaged by atomic force microscopy. *Circulation Research*, 74, 163-171.
- [54] Fung, Y. C. 1981. *Biomechanics, Mechanical Properties of Living Tissues*. Springer Verlag, New York.
- [55] White F. M. 1974. *Viscous Fluid Flow*. McGraw-Hill, New York.
- [56] Xue H. 2005. The modified Casson's equation and its application to pipe flows of shear thickening fluid. *Acta Mechanica Sinica*, 21, 243-248.
- [57] Selvarajan S., Tulapurkara E. G. and Ram V. V. 1998. A numerical study of flow through wavy-walled channels. *International Journal for Numerical Methods in Fluids*, 26(5), 519-531.
- [58] Brassur J. G. and Corrsin S. 1987. The influence of a peripheral layer of different viscosity on peristaltic pumping with Newtonian fluids. *Journal of Fluid Mechanics*, 174, 495-519.
- [59] Li M. and Brassur J. G. 1993. Non-steady peristaltic transport in finite-length tubes. *Journal of Fluid Mechanics*, 248, 129-151.
- [60] Higdon J. J. L. 1985. Stokes flow in arbitrary two-dimensional domains: shear flow over ridges and cavities. *Journal of Fluid Mechanics*, 159, 195-226.

